AFRL-SR-AR-TR-02-

0223

REPORT DOCUMENTATION PAGE

1. REPORT DATE (DD-MM-YYYY)	2. REPORT TYPE	3. DATES COVERED (From - To)
23-06-2002	Final Technical Report	November 2000 – November 2001

4. TITLE AND SUBTITLE

A Comprehensive Investigation of the Role of Vacuum Facility Pressure on High-Power Hall Thruster Testing

5a. CONTRACT NUMBER
F49620-01-1-0061

5b. GRANT NUMBER

5c. PROGRAM ELEMENT NUMBER

6. AUTHOR(S)

Alec D. Gallimore, Mitchell L. R. Walker, and Richard R. Hofer

5d. PROJECT NUMBER

5e. TASK NUMBER

5f. WORK UNIT NUMBER

7. PERFORMING ORGANIZATION NAME(S) AND ADDRESS(ES)

The University of Michigan
DRDA 3003 South State Street
Wolverine Tower, Room 1058
Ann Arbor, MI 48109-1274

8. PERFORMING ORGANIZATION REPORT NUMBER

9. SPONSORING / MONITORING AGENCY NAME(S) AND ADDRESS(ES)
AFOSR/NA
801 N. Randolph Street, Room 732
Arlington, VA 22203-1977

10. SPONSOR/MONITOR'S ACRONYM(S)
AFOSR

11. SPONSOR/MONITOR'S REPORT NUMBER(S)

12. DISTRIBUTION / AVAILABILITY STATEMENT
Approved for Public Release; Distribution Unlimited

13. SUPPLEMENTARY NOTES

14. ABSTRACT

Closed-Drift Hall thrusters (CDTs) have great potential in satisfying many of the spacecraft propulsion needs of the United States Air Force for the next several decades. Its combination of high specific impulse, high thrust efficiency, and high thrust density makes it very attractive for a number of earth-orbit missions. However, due to the wide range of facilities used in CDT testing, it is difficult for researchers to make adequate comparisons between data sets because of both dissimilar instrumentation and backpressures. Thus, a tool is needed that allows researchers to obtain relevant plume data for a variety of chambers and backpressures. To this end, our work for this one-year effort has focused on studying the effectiveness of collimated Faraday probes in obtaining ion current density profiles of CDTs. A collimated probe is attractive because it offers the possibility of obtaining the true ion current density profile regardless of facility pumping speed by filtering low-energy charge-exchange collisions ions from the collector. We compare the ion current density profiles obtained simultaneously with collimated and "nude" probes one meter from a CDT, at two facility pumping speeds and at thruster power levels between 1.5 and 5.0 kW.

15. SUBJECT TERMS
Hall Thruster, Electric Propulsion, Plasma Physics, Vacuum Facilities

16. SECURITY CLASSIFICATION OF: Unclassified			17. LIMITATION OF ABSTRACT	18. NUMBER OF PAGES	19a. NAME OF RESPONSIBLE PERSON
a. REPORT	b. ABSTRACT	c. THIS PAGE			Mitat Birkan
Unclassified	Unclassified	Unclassified	UU	59	19b. TELEPHONE NUMBER (include area code) NA (703) 696-7234

Standard Form 298 (Rev. 8-98)
Prescribed by ANSI Std. Z39.18

20020719 135

FINAL TECHNICAL REPORT

For research supported by
AFOSR Contract No. F49620-01-1-0061
for period 11/15/2000 to 11/14/2001

A Comprehensive Investigation of the Role of Vacuum Facility Pressure on High-Power Hall Thruster Testing

Prepared by

Alec D. Gallimore*, Mitchell L. R. Walker,[%] and Richard R. Hofer[%]

Department of Aerospace Engineering
University of Michigan
Ann Arbor, MI 48109

Work Supported by

Air Force Office of Scientific Research
Program Monitor: Dr. Mitat Birkan

---

* Associate Professor and Director of the Plasmadynamics and Electric Propulsion Laboratory
[%] Graduate Student Research Assistant

June 2002

Introduction

Propulsion systems having high exhaust velocities (Ve>10 km/s) are desirable for a variety of space missions. In order for a propulsive system not to require an inordinate amount of propellant, its exhaust velocity should be of the same order as or greater than the characteristic velocity increment (Delta-V) required for a given space mission. Studies have shown that for orbit transfer missions of interest by NASA and the DoD, a characteristic velocity increment of over six kilometers per second may be necessary.[1] Furthermore, experience gleaned from operation *Desert Storm* shows the need for military space assets to be rapidly repositioned without excessive use of onboard propellant; *i.e.*, the need for high specific impulse propulsion systems of moderate thrust.

Cryogenically-fueled chemical rockets, which rely on the intrinsic energy available from the chemical reactions of their constituent propellants, are inherently limited to exhaust velocities below 5 km/s.[2] Chemical rockets that use space storable propellants such as hydrazine are limited to exhaust velocities of about 3 km/s.[2] Thus, propulsion systems that produce exhaust velocities considerably higher than those obtained with chemical systems would greatly enhance a variety of orbital space missions.

Ideally, an engine that would be used as the primary source of propulsion for satellite station-keeping and orbit repositioning in modern spacecraft should produce an exhaust velocity between 10 and 25 km/s.[3] To achieve this performance, a propulsion system must accelerate its propellant gas without relying on energy addition through chemical reactions. One approach is the application of electrical energy to propellant in the form of electrical heating and/or electric and magnetic body forces. This type of propulsion system is commonly known as electric propulsion (EP).

EP can be categorized into three groups:[4] i) *Electrothermal Propulsion Systems* in which a gas is electrically heated, either with resistive elements or through the use of an electric arc, and is subsequently expanded through a supersonic nozzle to produce thrust; ii) *Electromagnetic Propulsion Systems* that use electromagnetic body forces to accelerate a highly-ionized plasma; and iii) *Electrostatic Propulsion Systems* that use electric fields to accelerate ions.

In addition to possessing suitable exhaust velocity, an EP system must also be able to convert onboard spacecraft power into directed kinetic power of the exhaust stream efficiently (*i.e.*, possess high thrust efficiency) and must generate suitable thrust to ensure reasonably short deployment times.

Electrothermal systems have limited utility for this role because of performance constraints placed on them by excessive frozen flow and electrode losses.[5,6,7] The specific impulse and thrust efficiency of arcjets operating on standard space-storable propellants (*e.g.*, hydrazine) is limited to less than 650 seconds and 41%, respectively. Recent Air Force arcjet tests have demonstrated specific impulses of over 800 seconds on ammonia. Steady-state electromagnetic systems have demonstrated high thrust efficiencies only at power levels that far exceed those generated onboard current or anticipated spacecraft.[8,9] Gridded electrostatic engines (*e.g.*, ion thrusters), which can achieve large exhaust velocities (Ve>50 km/s) at high thrust efficiencies

(>70%), have traditionally demonstrated efficient performance at exhaust velocities above 30 km/s,[4,10,11] that is beyond the desired range for orbit transfer missions.[3] The high specific impulse of the ion thruster means that for a given spacecraft power level, it will generate less thrust than a lower Isp counterpart, resulting in larger trip times and a demand for longer thruster life. Furthermore, ion thrusters pay a penalty for its high power processing specific mass due to its large operating voltages (*e.g.*, 1100 V) and are limited in thrust density by space-charge effects, making ion thrusters considerably bulkier than other EP systems.[4]

Therefore, the ideal propulsion system for orbit transfer missions and for satellite station-keeping is a compact engine of high thruster density that efficiently accelerates propellant (*e.g.*, through electrostatic means) to modest exhaust velocities while requiring discharge voltages of less than 1000 V. As is shown below, the Hall thruster is a device that fulfills these requirements.

The Hall Thruster

The Hall thruster is an electrostatic engine that was developed in the 1960s to alleviate the thrust density limitation of ion thrusters that results from space-charge effects within the acceleration volume. Hall thrusters were also attractive from the standpoint that since grids are not required to accelerate ions, they do not suffer from the large grid erosion rates of ion thrusters. Interest in the Hall thruster waned in the early 1970s, however, because of budgetary cuts and because American researchers were never able to demonstrate that these engines could operate at thrust efficiencies near those achieved with ion thrusters.[12,13,14] As such, Hall thruster research essentially disappeared in the U.S. between 1972 and 1985. From 1985 to 1990, Ford Aerospace (now Space Systems/Loral), in conjunction with the NASA Lewis Research Center (now the John Glenn Research Center at Lewis Field [GRC]), funded a small research effort to determine if Hall thrusters could be used for North-South station-keeping (NSSK).[15,16] This program proved to be unsuccessful and was abandoned.

Throughout this period, however, Hall thruster research flourished in the Soviet Union, ironically partly because Soviet engineers were never able to develop adequate grids for ion thrusters. Hall thrusters were first tested in space in 1971 with immediate success.[16,17] Since then, over one hundred Hall thrusters have been used on Soviet and Russian spacecraft, mostly as plasma contactors and for East-West station-keeping. However, in 1994 the first satellite to use Hall thrusters for NSSK was launched by Russia. Because of this and numerous experiments that show that Russian Hall thrusters are capable of generating exhaust velocities of 15 to 22 km/s (*i.e.*, specific impulses of 1500 to 2200 seconds) at thrust efficiencies of 50% or more,[18] there has been a great deal of interest in using these engines on American spacecraft for NSSK and for orbit repositioning. For example, the Ballistic Missile Defense Organization (BMDO) in conjunction with NASA GRC and the Naval Research Laboratory (NRL) developed a flight experiment that used a Russian Hall thruster on a U.S. experimental satellite.[19] Space Systems/Loral (SSL) has announced that its next generation of communication satellites will use Hall thrusters for NSSK, perhaps as early as this year (2002). Clearly this device, with performance far superior to that of arcjets, and which is better-suited for Earth orbit missions than gridded ion thrusters[1], currently the most advanced propulsion system used on American spacecraft, would not only serve as an excellent thruster for orbit station-keeping and

repositioning roles, but potentially could be scaled in power to propel orbit transfer vehicles and future planetary probes. Thus, GRC issued two contracts for the development of two-stage Hall thrusters with performance equivalent to that of the NSTAR ion thruster flown on NASA's 1998 Deep Space 1 mission. The University of Michigan recently operated its P5-2 Hall thruster at a discharge voltage above 1000 V for an exhaust velocity above 30 km/s.

The Closed-Drift Hall Thruster

There are two types of Hall thrusters that have been studied at great lengths; the end-Hall thruster and the closed-drift Hall thruster (CDT). Both engines, in principle, are capable of producing specific impulses in excess of 1500 seconds with xenon at a thrust efficiency of 50% or greater. However, it is the CDT, which has been developed and used in the former Soviet Union over the past forty years, that is of the most interest to the Western space technology community.

The CDT is a coaxial device in which a magnetic field that is produced by an electromagnet is channeled between an inner ferromagnetic core (pole piece) and outer ferromagnetic ring (Figure 1). This configuration results in an *essentially* radial magnetic field with a peak strength of a few hundred gauss. This field strength is such that only the electrons are magnetized. In addition, an axial electric field is provided by applying a voltage between the anode and the downstream cathode. As the electrons stream upstream from the cathode to the anode, the **ExB** action on the electrons causes them to drift in the azimuthal direction, forming a Hall current. Through collisions, these electrons ionize propellant molecules that are injected through the anode and which are subsequently accelerated by the axial electric field. The mixture of electrons and ions in the acceleration zone means that the plasma is electrically neutral, and as such, is not space-charge limited in ion current (thrust) density. Since the magnetic field suppresses the axial mobility of the electrons while exerting essentially no effect on ion dynamics, the plasma can support an axial electric field with a potential difference close to the applied voltage between the electrodes. Thus, the bulk of the ions are accelerated to kinetic energies to within 85% of the applied discharge voltage.[12] This combination of processes accounts for the CDT's high thrust efficiency.

Russian CDTs come in two variants; the stationary plasma thruster (SPT) (also known as the magnet layer thruster) and the anode layer thruster (TAL). The main difference between these two devices is that the SPT uses a dielectric coating that usually contains boron nitride to electrically insulate its acceleration channel walls while the TAL uses a much shallower channel made out of refractory metals. Performance characteristics of both engines are virtually identical. Although they vary in size and input power, CDTs that are currently being considered for NSSK typically operate at discharge voltages of 300 to 350 V, and thruster currents between 4.5 and 15 A, with xenon mass flow rates of 5 to 18 mg/s. As the discussion below will show, the power level (and therefore the current and mass flow rates) that will be needed in the near future will be considerably higher.

Motivation

High-Power Electric Propulsion

Communication satellites are becoming both larger and more powerful. This fact is acknowledged throughout the EP community. Hughes Corporation's recent development of the HS-702 satellite with up to 15 kW of solar array power and SS/L's announcement of the 2020 spacecraft with more than 20-25 kW of solar array power by 2003 (nearly twice the power available from today's largest communication satellite) suggests that EP systems will also have to double (or triple) in power from the current 1-3 kW systems within the next decade to satisfy commercial spacecraft. This means that vacuum systems will have to be modified to handle the added propellant flow rates demanded by these higher-power thrusters. The Air Force Research Laboratory (AFRL), GRC, and the Jet Propulsion Laboratory (JPL) have recently upgraded their pumping systems in anticipation of the higher-powered thrusters. Moreover, the fact that the major emphasis of the DoD Integrated High Payoff Rocket Propulsion Technology (IHPRPT) program in EP was on high-power CDTs suggests that the United States Air Force (USAF) acknowledges the importance of high-power engines for its future.

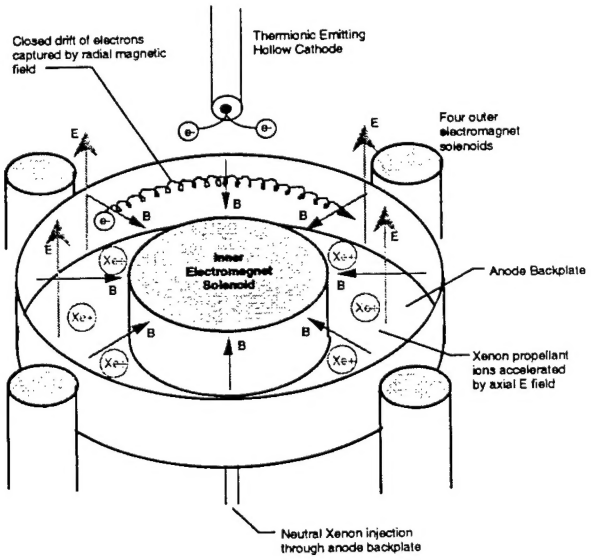

Figure 1 — Schematical diagram of a closed-drift Hall thruster.

USAF Interest in High-Power Electric Propulsion

With the end of the Cold War, the landscape of global conflict has changed immensely. No longer is surveillance over a fixed region (*e.g.*, the former Soviet Union) adequate for intelligence gathering. Today's intelligence gathering spacecraft must be made more maneuverable and hence easier to re-deploy to be able to respond to a crisis at a moment's notice. After the DoD lost hundreds of millions of dollars of space assets during the Gulf War when

reconnaissance satellites ran out of propellant after rapid re-deployment over the Gulf, the DoD – and the USAF in particular – became committed to using advanced propulsion on their spacecraft. In its recent study entitled "Air Force New Vista 2020," which looked ahead some twenty-five years to predict the future roles and capabilities of the Air Force, the Air Force Scientific Advisory Board listed electric propulsion as one of the key technologies that must be used routinely by the 21st century Air Force.

With the USAF's desire to develop higher-power, more capable spacecraft for radar-based remote sensing, optical imaging, weather tracking, and communication comes the need for high-performance medium- (2–5 kW) and high-power (6-10 kW) EP systems for station-keeping and repositioning. However, the USAF has recently determined that even more powerful CDTs systems (*e.g.*, 20-50+ kW) will be needed for a variety of missions in the not-so-distant future. These missions include propulsion for orbital transfer vehicles (OTVs), space tugs, and high-power space-based radar and laser systems. The recent multi-million dollar award given by the USAF to an industrial team comprised of SS/L, Atlantic Research Corporation, and the Russian design bureau Fakel, under the IHPRPT program, for the development of the 5-kW-class SPT-140 CDT attests to the importance of this technology to the defense community. And yet, while the evolutionary path for scaling current 5-kW-class CDTs to 50 kW is uncertain because of a variety of scaling issues, it is clear that testing 50-kW-class CDTs in current or expected test facilities poses a challenge.

The reason for this is that as thruster power is increased, its internal discharge chamber pressure tends to decrease to maintain efficient operation. However, thruster mass flow rate, and hence facility background pressure, increases proportionately with power. So as the power of the CDT increases, its internal pressure decreases and yet the background chamber pressure increases. This poses an issue not only for measuring high-power CDT performance and plume/contamination characteristics, but also for assessing engine life during lifetests.

To show this, we must first look at how thruster parameters scale with power, what the ideal pressures are to evaluate thruster performance, plume/contamination characteristics, and life, and why it is likely that high-power CDTs will have to be developed with test-facilities with less than ideal pressures.

CDT Scaling Laws and Consequences for Testing

A CDT must adhere to several scaling laws in order to operate efficiently. While several researchers in Russia and the U.S. have developed CDT scaling laws[12,1720,21] there is not universal agreement among them. However, these models all tend to reflect the following design trends, assuming that the CDT is geometrically scaled in size such that a characteristic length, L (usually considered the width between the inner and outer discharge chamber walls), exists and the voltage (*i.e.*, specific impulse) is fixed;

$$B \sim 1/L \quad (1)$$

$$P \sim 1/L \quad (2)$$

$$J \sim L \quad (3)$$

where B is the magnetic field strength, P is the discharge chamber pressure, and J is the discharge current. Thus, according to these scaling factors, a high-power CDT: (1) must be physically larger since J and hence power (for fixed discharge voltage) scales with L; (2) must operate at a lower chamber pressure to ensure that adequate ionization is maintained throughout the discharge chamber; and (3) requires a smaller magnetic field to provide adequate electron confinement. The inverse relation between B and L can also be derived by considering the magnetic integral, (integral of Bdx where x is the axial coordinate) a quantity that has been shown to be a good similarity parameter for CDTs. [Note: Use of this quantity as a scaling parameter also comes from assuming that Bohm cross-field electron diffusion processes are at play in CDTs, something that has been shown to be true by experiments.[12]]

Figure 2 shows a plot of thruster power as a function of thruster size (discharge chamber outer diameter) derived from the referenced scaling laws. Also shown in the figure are CDTs developed by the Fakel design bureau in Russia (SPT series of thrusters) and the successful P5 laboratory-model CDT developed at The University of Michigan and AFRL. The figure shows that there is excellent agreement between the model and engines developed up to the 25 kW power level. Extrapolated engine sizes for 25-50 kW are shown as well. We note that the discharge chamber diameter does not increase linearly with power as the scaling laws above (Equations (1)-(3)) would suggest because the scaling length is usually chosen as the channel width.

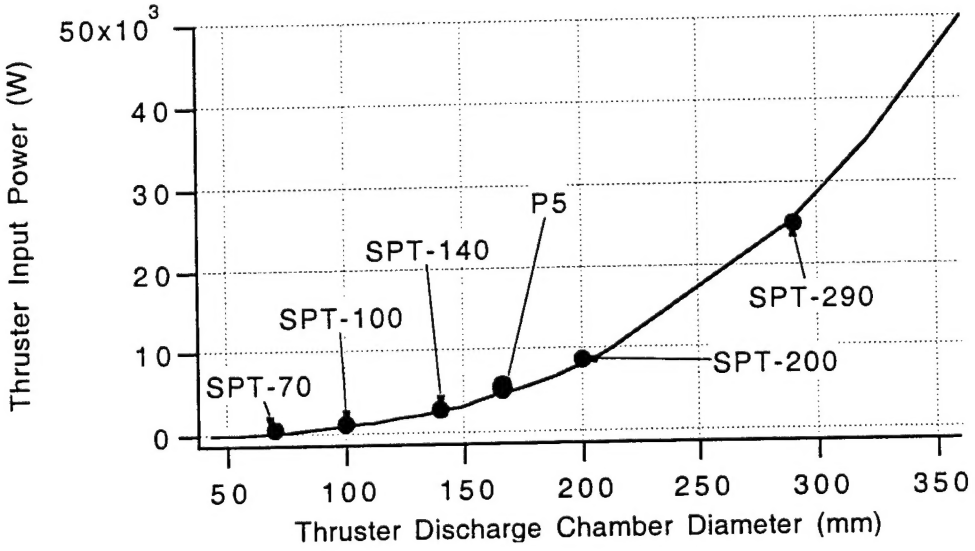

Figure 2 — Thruster power vs. discharge chamber diameter

The same scaling model used to generate Figure 2 was used to estimate the pressure within the discharge chamber of a CDT (Figure 3). While medium-power (1-5 kW) CDTs are predicted to have pressures of about $5\text{x}10^{-4}$ Torr—which is consistent with measurements[22] and modeling[23]—a 50 kW CDT will have chamber pressures a factor of five lower; i.e., approaching

$1x10^{-4}$ Torr. Thus, the internal pressure of 50 kW CDTs will approach the background pressure that many of today's test facilities can maintain with 5 kW thrusters. The importance of minimizing facility effects by maintaining a low background pressure and large internal chamber volume will be reviewed in the next subsection.

The Influence of Facility Effects on Thruster Testing

Although CDTs have performance characteristics that make them attractive for Earth-orbiting missions, the complex nature of their operation is a source of concern from a spacecraft integration point-of-view. For example, CDTs that use dielectric channel coatings suffer from excessive insulator erosion. Much of this erosion is due to sputtering from energetic ions near the exit of the discharge chamber. TALs, on the other hand, which erode metal from its channel walls, may pose an even more serious threat to spacecraft health (*e.g.*, to the solar arrays). Such erosion poses a potential hazard to spacecraft operation since ablated insulated material could coat vital spacecraft surfaces like solar arrays and optics.

In addition, there is further concern that the spacecraft could be damaged by side or back-scattered exhaust ions. The ions accelerated by the thruster travel at kinetic energies in excess of 250 eV.[24] Since a non-negligible fraction of the exhausted particles travel at angles in excess of 45° from the thruster axis, plume divergence not only detracts from engine performance, but also results in damage to the spacecraft due to sputtering.

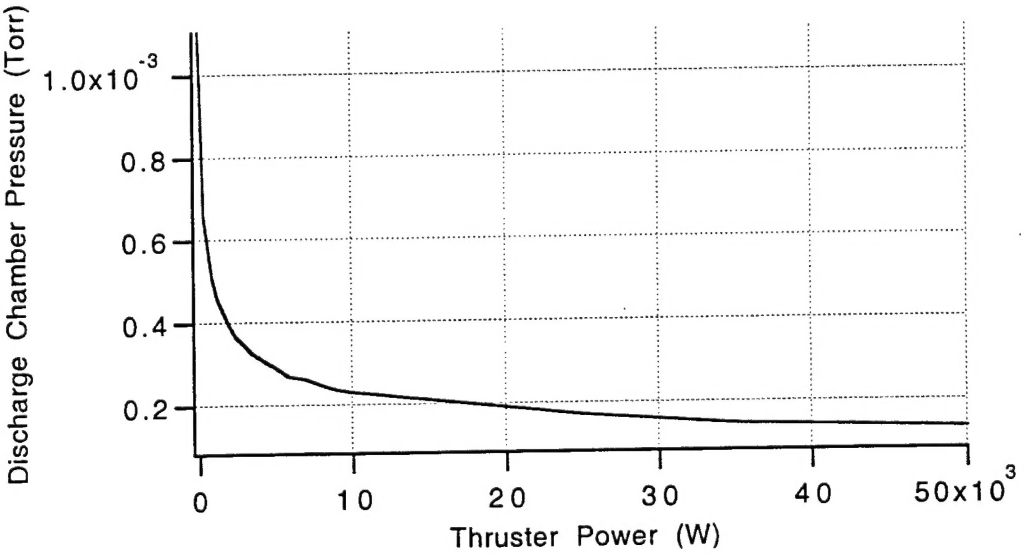

Figure 3 — Discharge chamber pressure as a function of thruster power

The erosion/deposition characteristics in the plume of CDTs are quite complex. Experiments have shown that in the central region (45°) of the plume, the energetic ions tend to remove deposited materials from structures in such a way that the net erosion rate overwhelms the surface deposition rate of thruster effluent material.[25] At higher angles with respect to the thruster axis of symmetry, however, the opposite is true: That is, the plume tends to remove material from objects placed near its axis of symmetry, and deposits matter on objects at higher

angles.[25] The exact location where this transition occurs (and what parameters it may depend on) remains unknown.

What complicates the endeavor of characterizing the above processes is the fact that facility effects can have a profound impact on these measurements. Improper matching of an engine and test goals with a facility can render a series of experiments meaningless. For example, if the chamber is too small, its boundaries (walls) can affect measurements by altering the flowfield or by introducing contaminants due to tank wall erosion. Material sputtered from tank walls can interfere with measurements that use witness plates, collimated samples, and QCMs to predict thruster and spacecraft material erosion. The electrical conductivity of tank walls has been shown to influence the electric field in the plume and the plume flow field.[26]

If the tank pressure is too high, the background gas can artificially modify the exhaust plume as well as alter the operation of the CDT itself. Thruster operation may be influenced by entrainment and/or ingestion of the background chamber molecules. This effect artificially increases the propellant mass flow rate of the engine, resulting in performance and operation changes consistent with the increased number of propellant particles. Furthermore, plume diagnostic experiments can be affected. A large partial pressure of background gas molecules can affect ion current density and energy distribution measurements by artificially increasing the local charge density through charge exchange collisions. For example, at large angles from the CDT axis, the ion energy distribution profile is dominated by low-energy charge exchange ions, the source of which is thought to be background gas; although neutral particles emanating from the cathode and thruster discharge chamber could be responsible as well.[18,23,26]

Randolph *et al.*[25] suggest that in order to characterize a CDT in terms of performance, electromagnetic interference (EMI), far-field (~1 m) plume properties (and hence spacecraft contamination), and life (and hence erosion and contamination characterization), the vacuum chamber pressure should be no more than $5x10^{-5}$, $5x10^{-5}$, $1.2x10^{-5}$, and $5x10^{-6}$ Torr, respectively. Since the pressure at low Earth orbit and at Geosynchronous orbit are approximately $5x10^{-6}$ and $5x10^{-10}$ Torr, respectively, a perfect simulation of pressure is not always necessary. Randolph based his analysis on free-molecular flow, arguing that below a certain chamber pressure, thruster operating characteristics are not affected by the random flux of particles. Conversely, if a thruster is tested above the specified pressure, the influence of background gas being ingested into the engine through free-molecular flow must be taken into account when analyzing test data. However, since Randolph based his pressure estimates on 1-kW-class thrusters where the internal pressure is expected to be approximately $5x10^{-4}$ Torr, it stands to reason that still lower pressures would be needed for high-power thrusters where internal pressures are lower. If we conserve the ratio of thruster chamber pressure and tank pressure, we find that Randolph's estimates may be a factor of five too high for 50 kW engines. This is reflected in Table 1 that shows Randolph's original criteria for 1-kW-class thrusters, and the modified criteria for 50-kW-class CDTs.

As the table shows, chamber pressures between $1x10^{-6}$ and $1x10^{-5}$ Torr are needed to characterize high-power CDTs. To compare these pressure criteria to what is achievable on the ground, Figure 4 shows the background pressure of three large national electric propulsion vacuum facilities (*i.e.*, facilities not owned and operated by corporations) as a function of thruster power. These facilities include the Large Vacuum Test Facility at the University of Michigan (xenon

pumping speed of 245,000 l/s), AFRL's Chamber 3 (350,000 l/s), and NASA Glenn Research Center's Tank 5 (1,000,000 l/s). The CHAFF-IV facility, with a predicted xenon pumping speed of 9,000,000 l/s,[27] was excluded from this chart because it is currently under development at USC. As the figure clearly shows, none of the national test facilities shown can maintain an adequately-low background pressure to satisfy Randolph's pressure criteria. This fact was echoed recently both in a talk at the 35th Joint Propulsion Conference given by Robert Jankovsky of NASA GRC and at an AFOSR workshop on space-based electric propulsion testing in Norfolk, Virginia in 1999. Given the cost of adding pumping speed to a facility—between $1 and $4 per l/s—and the fact that most facilities are filled to capacity with cryosurface area already, it is unlikely that a factor of ten or more improvement in pumping speed will take place by the time 50 kW CDTs are being developed.

Table 1 — Required chamber pressure as a function of CDT test activity from the analysis of Reference[25] for 1-kW- and 50-kW-class CDTs (300 V assumed).

CDT Test Activity	**Desired (1 kW) Pressure (Torr)**
Performance	5×10^{-5}
EMI	5×10^{-5}
Plume/Contamination	1×10^{-5}
Life/Erosion	5×10^{-6}
CDT Test Activity	**Desired (50 kW) Pressure (Torr)**
Performance	1×10^{-5}
EMI	1×10^{-5}
Plume/Contamination	2×10^{-6}
Life/Erosion	1×10^{-6}

Randolph shows that tank design, in addition to tank pressure, plays a role in assessing thruster performance, plume characteristics, and life since the amount of sputtered tank wall material that deposits on thruster surfaces depends on the geometry and size of the vacuum chamber.

In terms of chamber size, one could argue that since the characteristic length of a typical satellite is between 1 and 10 m, the chamber should be of this size as well in order to make realistic plume measurements at a location from the exit plane that is representative of the distance actual flight hardware components are likely to be placed with respect to EP thrusters. Furthermore, the chamber should be as close to a sphere as possible with the thruster operating in the center so that a complete study of the plume can be made in all directions and to maximize the path length that sputtered wall material must travel to the thruster. Both of these assertions are corroborated by Randolph's analysis that suggests that a cylindrical chamber with a length-to-diameter ratio of

1.2 (*i.e.*, close to spherical) and a characteristic length of several meters is optimum.[25] All of the national facilities referenced in Figure 4 satisfy these criteria. Moreover other facility concerns associated with testing high-power thrusters (*e.g.*, vacuum seal thermal loading) can be addressed with straight-forward facility engineering such as water-cooled graphite beam dumps.

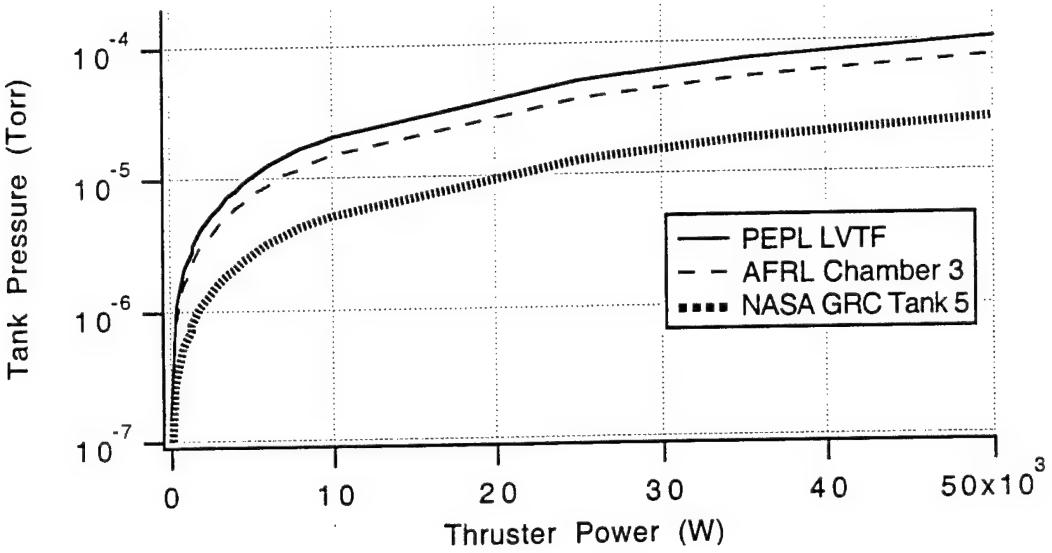

Figure 4 — Vacuum chamber pressure vs. thruster power for University of Michigan Large Vacuum Test Facility (240 kl/s), AFRL Chamber 3 (350 kl/s), NASA Glenn Research Center Tank 5 (1,000 kl/s). All pumping speeds are for xenon.

The message from this section is that national electric propulsion test facilities, while large enough to test 50 kW thrusters, posses pumping speeds that are at least an order of magnitude too low to ameliorate facility pressure effects for plume/contamination and life testing. As such, corrective measures must be developed to interpret test results in elevated chamber pressures.

Summary of Proposed Research Effort

Research Proposal Summary

CDTs have great potential in satisfying many of the spacecraft propulsion needs of the USAF for the next several decades. Its combination of high specific impulse, high thrust efficiency, and high thrust density makes it very attractive for a number of earth-orbit space missions. The USAF has recently identified the high-power (*e.g.*, 20-50 kW) CDT as an attractive propulsion system for future missions. These missions include propulsion for orbital transfer vehicles (OTVs), space tugs, and high-power space-based radar and laser systems. While the evolutionary path for scaling current 5-kW-class CDTs to 50 kW is uncertain because of thermal loading issues, plume neutralization matters, and overall scaling concerns, it is clear that testing 50-kW-class CDTs in current or expected test facilities is an issue, as was shown above. The

reason for this is that as thruster power is increased, its internal discharge chamber pressure tends to decrease to maintain efficient operation. However, thruster mass flow rate, and hence facility background pressure, increase proportionately with power. So as the power of the CDT increases, its internal pressure decreases and yet the background chamber pressure increases. This poses an issue not only for measuring high-power CDT performance and plume/contamination characteristics, but also for assessing engine life during lifetests.

Given the fact that an order-of-magnitude increase in pumping speed would be necessary to satisfy pressure requirements, it is likely that high-power CDTs will have to be developed with test-facilities with less than ideal pressures. The solution to this dilemma is to develop tools to correct for facility effects when making performance, plume, and lifetime measurements. While the ultimate tool may be numerical in nature, a great deal of basic measurements need to be made to help develop this design tool and to validate it. Moreover, much can be gained by developing operating procedures or simple correction factors to take into account facility effects.

To this end, we offered a proposal to address this issue in a three-year program. Our program will:

- Characterize how thruster performance is affected by facility pressure;
- Determine how chamber pressure influence beam divergence, ion energy distribution, plume ionization state, and the transport of contaminants (*e.g.*, thruster erosion products);
- Investigate what role chamber pressure has on thruster erosion and engine life; and
- Collaborate heavily with Professor Iain Boyd, an expert in plume modeling, who will dedicate a scholarship graduate student to support this work through modeling.

Our goal was to provide insight on how chamber pressure influences these engine characteristics. We believe such insight is necessary before design/testing tools can be developed.

- We used the 5-kW-class P5 laboratory-model thruster (see Experimental Facilities Section), developed under AFOSR funding, as the test bed for this investigation. Though designed to operate at 15 A – 300 V, the P5 was operated at low current (~5 A) to simulate the low internal pressure of a 50 kW CDT. Given its size (equivalent to an "SPT-170") in comparison to other thrusters of this power class,[21] the P5 was expected to be able to operate up to ~8 kW (it exceeded 9 kW in one test).

All testing were performed in the 6-m-diamter by 9-m-long Large Vacuum Test Facility (LVTF). This cryopumped facility will be capable of a xenon pumping speed of over 240,000 l/s now that three internal cryopumps were added to the four currently in operation (see Experimental Facilities Section). This modular cryopumping system enables any combination of the seven cryopumps to be operated, resulting in a wide range of background pressures for a given thruster power level (see Figure 5).

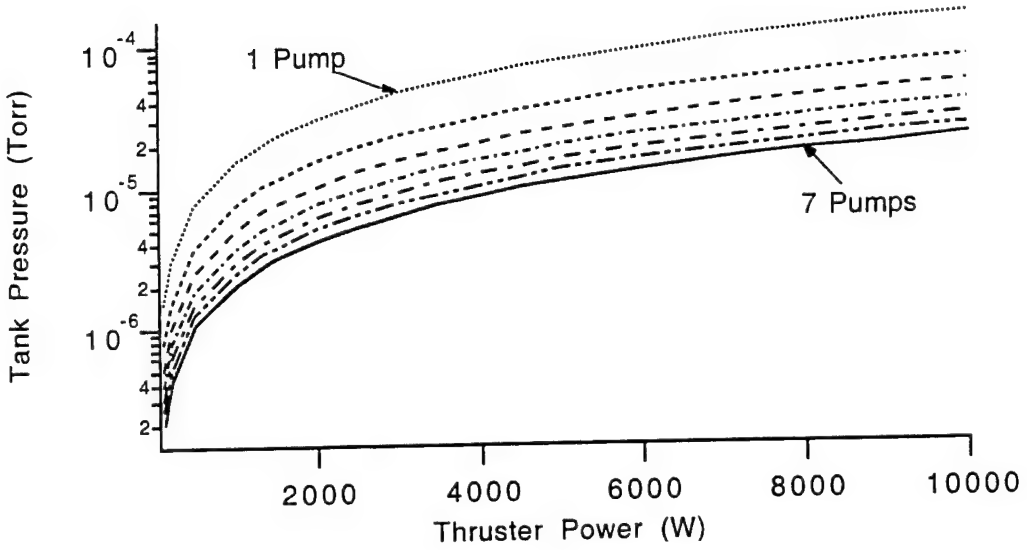

Figure 5 — LVTF Pressure as a function of thruster power (@ 300 V) with 1 - 7 pumps on.

Year 1 Accomplishments

Our efforts to date on this grant have concentrated on five areas: 1) extending the state-of-the-art in plume diagnostics; 2) performance characterization at multiple chamber pressures; 3) Laser-Induced Fluorescence (LIF) measurements of the P5 Hall thruster in preparation for Hall thruster insulator erosion measurements; 4) Internal characterization of Hall thruster magnetic fields, and 5) supporting AFRL experiments on a Busek Hall thruster cluster.

Plume Characterization

A shortcoming of conventional ("nude") Faraday probes is that the measured ion current density depends partly on the facility size and operating pressure. This makes for questionable comparisons between ion current density data collected in different chambers, almost all of which differ considerably with respect to tank size, shape, and pumping speed. These differences are most often driven by resonant charge exchange (CEX) collisions of directed plume ions with the random background population of neutrals. In resonant CEX collisions, a "fast" moving ion exchanges an electron with a "slow" moving neutral. Because the process does not involve momentum transfer, the resulting products are therefore a fast neutral and a slow ion with a random velocity distribution. CEX collisions have been shown by Manzella[28] to largely affect the measured current density profiles at angles greater than 30 degrees from thruster centerline. The goal of this work was to determine if collimated Faraday probes could be used to ameliorate the effect of spurious current from low-energy ions created in resonant CEX collisions. This additional current artificially increases beam current, particularly at large

off-axis angles (the region of the plume of most interest), and renders tank-to-tank comparisons difficult at best.

The collimated probe that was used for this study is based on the design developed by de Grys *et al.*[29] Figure 6 shows the basic geometry and a picture of the device. A standard "nude" Faraday cup (of diameter *Dcup*) is placed on the downstream side of the probe. The collimator filters low-energy CEX ions by being allowed to float or by being biased -20 V with respect to ground (-30 V with respect to the ambient plasma). The geometrical filtering of both high- and low-energy ions by the collimator must be accounted for. The collimator essentially images a spot of the thruster onto the Faraday cup. Hofer *et al.*[30] provide a detailed overview of the complicated analysis that corrects for the diminished field-of-view. It is very important that the neutrals created inside the collimator through the neutralization of beam and CEX ions are allowed to vent adequately in order to prevent a build-up of pressure. Increased pressure within the collimator would change the trajectory (and through CEX collisions, the charge state) of incoming beam ions. Thus, analysis was performed to ensure that adequate venting was provided. Our calculations predict that the pressure inside the collimator never exceeds the background pressure of the vacuum chamber.[30]

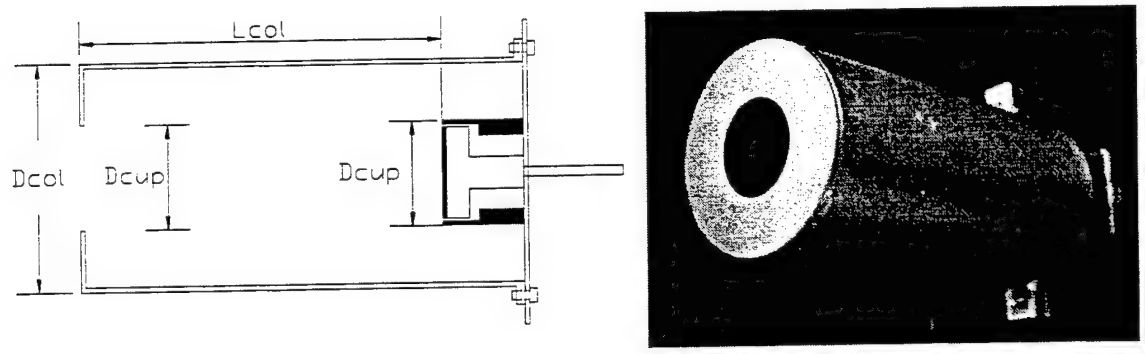

Figure 6 — Cross-sectional view and picture of the collimated Faraday probe. Venting is through both the entrance aperture and the space in the rear not occupied by the nude probe. The narrow crossbar holding the Faraday cup in place is shown.

Reference 30 provides a detailed review of the exhaustive study we performed with this collimated probe. We investigated the effect of guard ring bias voltage for both the nude and collimated probe, and the effect of collimator bias voltage (including floating voltage) on ion current data. Our experiments were performed with the new P5-2 thruster, which has a design similar to the P5.# The P5-2 incorporates a more advanced magnetic field design, and innovations such as a trim coil and a lanthanum hexaboride (LaB_6) auxiliary electrode for enhanced propellant ionization. A detailed description of the P5-2 can be found in Ref. [31]. These tests were performed in the Large Vacuum Test Facility (LVTF) at the University of Michigan Plasmadynamics and Electric Propulsion Laboratory (PEPL). Two AFOSR DURIP grants were used to replace the six oil diffusion pumps originally installed on the LVTF when it was built in the early 1960s with seven internal cryopumps. The seven internal cryopumps,

developed under AFOSR-sponsorship

which are equivalent to fourteen large cryotubs in terms of pumping speed, provide a xenon pumping speed of ~245,000 l/s; ten times the pumping speed that the six oil diffusion pumps provided for xenon. Table 2 summarizes the P5-2 operating conditions employed in this study.

Table 2 — P5-2 operating conditions.

V_d (V)	I_d (A)	Anode Flow (mg/s)	Cathode Flow (mg/s)	I_{im} (A)	I_{om} (A)	$V_{c\text{-}g}$ (V)	Pressure (Torr-Xe)	Bias (V)	Biased or Floating Guard Ring?
300	4.44	5.25	0.76	1.74	1.24	-25.7	3.4E-06	-20	Floating
300	4.46	5.25	0.76	1.74	1.24	-25.8	3.4E-06	-20	Biased
500	4.56	5.33	0.76	2.50	2.00	-21.7	3.4E-06	-20	Floating
500	4.56	5.33	0.76	2.50	2.00	-21.3	3.4E-06	-20	Biased
300	9.87	10.01	0.76	3.49	2.51	-23.8	5.7E-06	-20	Floating
300	9.87	10.01	0.76	3.49	2.51	-23.2	5.7E-06	-20	Biased
500	10.13	9.91	0.76	4.51	3.80	-22.4	5.7E-06	-20	Floating
500	10.04	9.91	0.76	4.51	3.80	-22.8	5.7E-06	-20	Biased

Figure 7 shows sample data comparing ion current density profiles collected with both a nude and collimated Faraday probe with the P5-2 Hall thruster operating at 5 kW. The background pressure was 5.7 x 10^{-6} Torr (Xe). The figure shows that the collimated probe profile is narrower, especially along the plume wings (angles greater than 45 degrees). This is expected since low-energy CEX ions are being collected by the collimator and not the Faraday cup. The collimated probe profile agrees in general shape with numerical predictions of Hall thruster current profiles in space where CEX ions are scarce. While we would expect the peak current density for a collimated probe to be lower than that of a nude probe due to CEX ion filtering, the measured decrease (38%) is greater than expected. We have ruled out CEX and elastic collisions within the collimator as the cause for the decreased current. While a radial electric field could account for this decrease by deflecting beam ions enough for them to miss the cup, the radial electric field for the case shown in Fig. 7 would have to be 3500 V/m, which corresponds to a collimator wall to centerline voltage drop of some 80 volts. While it is possible that our geometric correction model is not accounting for enough beam ions, we are quite confident that our approach is sound. Thus, we will perform the following to try to resolve this issue: 1) internal probing of the collimated probe to measure plasma potential, temperatures, and number densities; 2) study one combination that was not tested in Ref. [30]; float the collimator while biasing the guard ring and collector. This combination might mitigate the effects of the collimator on the plasma while still ensuring a flat sheath over the collector.; and 3) use a numerical code to analyze the particle flow in the probe. Appendix A reviews the entire study.

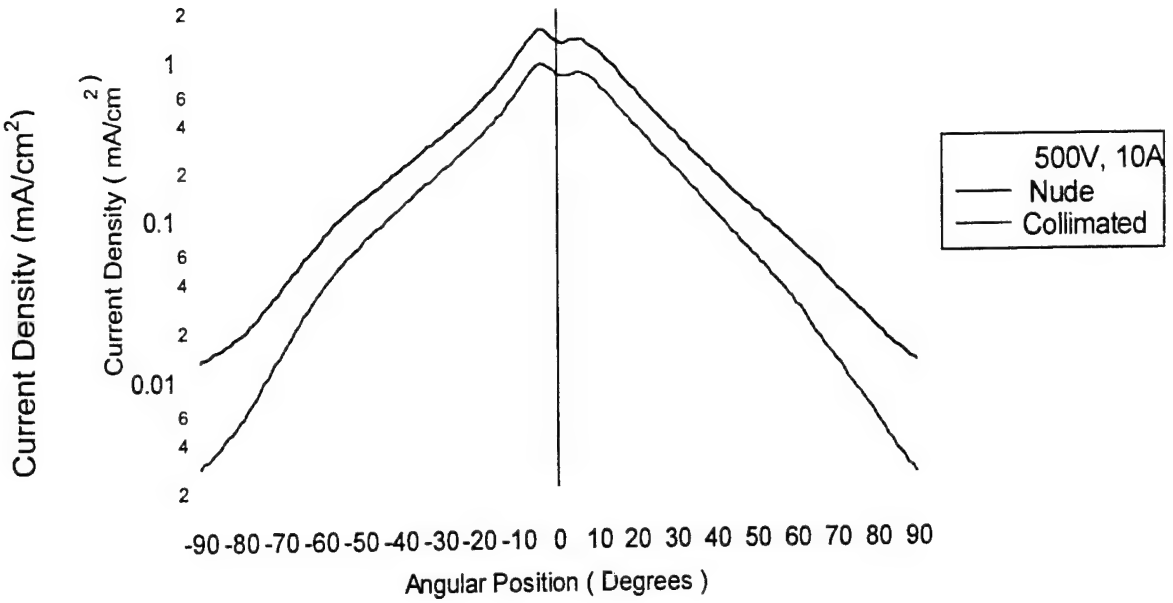

Figure 7 — Ion current density versus position for a nude and collimated probe.

Axial LIF

We have developed a new periscope axial laser delivery system to increase the accuracy of our LIF measurements. This approach replaces the multi-plex system we have been using for the past three years and improves the accuracy in measuring ion velocity and temperature from approximately 20% error to better than 1% precision error. We have also compared the ion energy distributions measured with the MBMS# and with LIF and have found the two techniques to agree with each other.[32] A detailed summary of the axial LIF work with the P5 thruster is provided in Reference [33].

Self-Magnetic Field

We have used the High-Speed Axial Reciprocating Probe (HARP) system,# in conjunction with a magnetic induction (Bdot) probe to characterize the vacuum and discharge magnetic fields of the P5 Hall thruster. The Bdot probe was found to agree with measurements made in table-top experiments with a NIST-traceable Hall probe both with a Helmholtz coil calibration rig, and with the P5 magnets operating both in air and in vacuum immediately after the thruster was turned off; *i.e.,* while the magnetic circuit was still warm. The Helmholtz coil was fitted with biased parallel plates to simulate the steady and time-varying (*e.g.,* 15 kHz) electric fields within the Hall thruster. The vacuum field was found to differ from the discharge field along discharge chamber centerline and near the outer wall of the thruster. By integrating the **JxB** Lorentz force to estimate thrust, where the Hall current was measured by Haas[34],# and the magnetic field was mapped by Peterson[35],# we were able to recover the thrust that was measured with a thrust stand.[36]

---

developed under AFOSR sponsorship

TWSLIF

We are setting up experiments in our Cathode Test Facility to conduct Two-Wavelength, Simultaneous LIF (TWSLIF) measurements to characterize discharge chamber erosion. We have successfully made LIF measurements with our second laser—the tunable diode laser purchased with our most recent AFOSR-DURIP grant—and we are in the process of configuring the optics to allow two separate sets of laser beams—one from the dye laser and one from the diode laser—at different wavelengths to interrogate a spot inside the CTF. Once this is established, we will use a calibrated ion sputtering source that was purchased with AFOSR-DURIP funds to erode a boron nitride substrate. Once the proof-of-concept experiment is completed, the graduate student will remain as a Post-Doc to port this technique over to the LVTF with an actual Hall thruster.

Performance

A comprehensive investigation of the effect of background chamber pressure on thruster performance is presented in Reference [37]. These experiments were conducted with the P5 Hall thruster at two LVTF pumping speeds—four pumps (140,00 l/s), and seven pumps (245,000 l/s)— at thruster power levels between 1.6 kW and 9.3 kW. Varying chamber pumping speed to study tank pressure effects is superior to elevating chamber pressure by auxiliary gas injection from a standpoint of cost (if xenon is used as the auxiliary gas), and by avoiding issues associated with where in the facility the auxiliary gas is introduced and what influence non-xenon auxiliary gas (to reduce cost) has on thruster operation. Our findings suggest that the standard assumption that people make to correct for facility effects—namely, that thrust remains constant with beam current and voltage—may not be true for all thrusters over all chamber pressures.[10]

Cluster Work

A PEPL student—Brian Beal—has spent several months at the Air Force Research Laboratory working with Dr. Bill Hargus and Dr. Greg Spanjers on conducting triple Langmuir probe measurements in the plume of a 2x2 Busek Hall thruster cluster. The work to date has found that the thrusters do interact with each other during operation and simply applying a single-engine plume prediction code to a cluster may not capture the subtle interaction of ion beams emanating from clustered engines. The student will return to Michigan in the Fall to design and build a new energy analyzer that will be employed to characterize the plume of the cluster. In 2002, the Busek cluster is slated to be sent to PEPL for plume and performance characterization. The LVTF has approximately an order of magnitude higher pumping speed that Chamber 6, the AFRL tank where the cluster is now operating. We recently submitted a proposal to the AFOSR DURIP to purchase a 2x2 Busek cluster and to perform the facility modifications necessary to allow for Cluster operation in the LVTF. Now that the DURIP grant has been awarded, the Busek cluster should arrive by November of 2002. A second P5 Hall thruster is being built to serve as the second half of a 2x1 P5 Hall thruster cluster at PEPL. The new P5 thruster will be delivered to PEPL in August, 2002.

Experimental Facilities

Plasmadynamics and Electric Propulsion Laboratory (PEPL) Vacuum Facility

A critical requirement for the proposed capability is to have a vacuum facility of high pumping speed and sufficient volume to minimize facility effects. This will be more important and difficult to achieve as thruster size and power continue to increase. The proposed investigation will take place in PEPL's 6-m-diameter by 9-m-long Large Vacuum Test Facility (LVTF) that has been used extensively for diagnostics of electric propulsion devices (Figure 8). The LVTF underwent a facility upgrade in 1998 wherein four CVI-TM1200 internal cryopumps were installed to replace the oil diffusion pumps previously used. The cryopumps give the LVTF a measured xenon pumping speed of 140,000 l/s. The base pressure of the LVTF is approximately $2x10^{-7}$ Torr. The LVTF maintains a pressure in the mid 10^{-6} Torr range (xenon pressure) during operation of the P5 thruster at medium power (1.3-kW) and the high 10^{-6} Torr range at 5 kW. A louvered 1.8 m by 1.8 m graphite beam dump is located on the center of the endcap downstream of the engine to minimize deposition of back-sputtered material from the bare tank wall. The thruster is always operated at least 4 m from the beam dump. An Air Force DURIP grant was used to add three TM1200 cryopumps to the LVTF in September of 2000 for a xenon pumping speed of 240,000 l/s on xenon.

P5 Closed-Drift Thruster

The thruster that will be used for this work is the PEPL/AFRL P5 5-kW-class laboratory model CDT (Figure 9). This engine was designed at PEPL and built at AFRL. The P5 was developed specifically for diagnostic access to the discharge chamber. The thruster has features associated with commercial SPTs including anode screens for magnetic field shaping. Compared to smaller thrusters, the P5 provides a larger discharge chamber for improved spatial resolution for optical measurements and electrostatic probes, as well as a lower power density (by virtue of thruster scaling) to reduce heat flux to probes. Thrust, specific impulse, and efficiency have been characterized thoroughly and have been reported along with plasma parameter profiles in the plume. The performance of this engine is equivalent to many commercial engines. The P5 has been operated at currents between 5 and 15 A and voltages up to 600 V. While designed for 5-6 kW, the P5 has demonstrated steady operation at 1.35 kW and is expected to be able to operate up to 8 kW given its size (equivalent to an "SPT-170") in comparison to other thrusters of this power class[21]. The P5 performance, interior plasma, and plume characteristics is also being extensively modeled by Professor Iain Boyd of the University of Michigan and his students.

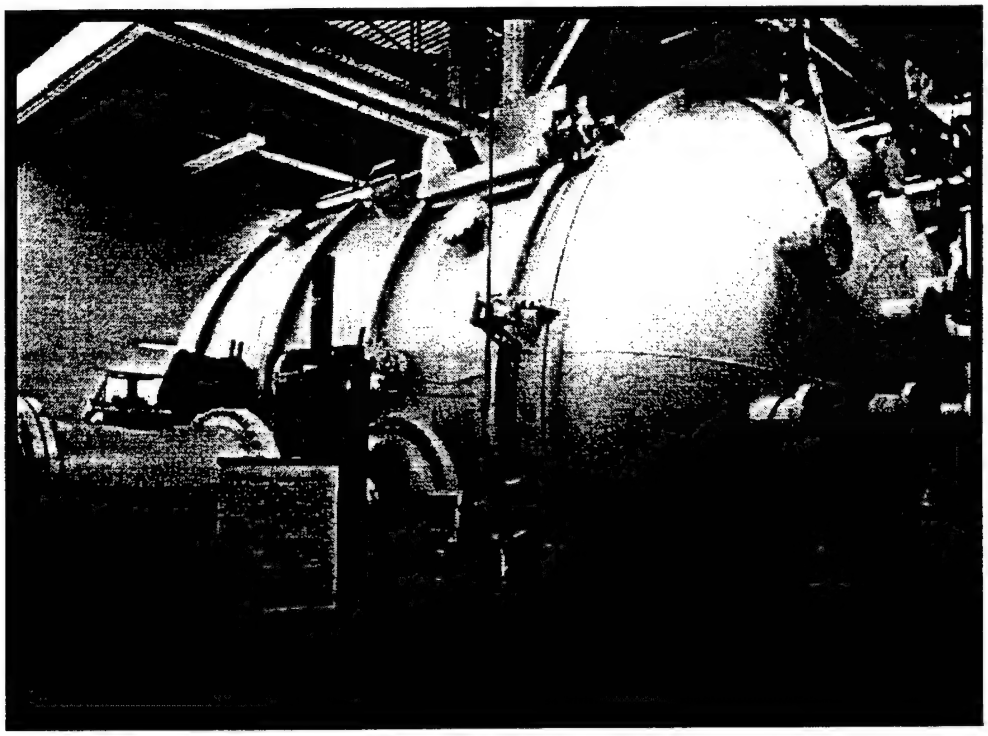

Figure 8 — The main vacuum chamber of PEPL - the Large Vacuum Test Facility (LVTF). This 9-m-long by 6-m-diameter chamber is supported by seven large TM1200 internal cryopumps, bringing its air and xenon pumping speed up to 525,000 l/s and 245,000 l/s, respectively.

PEPL Laser and Probe Facility

An argon-ion pumped Coherent ring-dye laser will be used for this project. The Coherent model 899-29 Autoscan II ring-dye laser is capable of outputting light within a spectral range of 375 nm - 900 nm (with appropriate dyes) with a linewidth of less than 500 kHz rms. The single frequency ring laser is computer controlled and has a wavelength meter attached to it which measures the laser frequency to within ±200 MHz (0.0067 cm^{-1}). The dye laser is pumped by a Coherent Sabre R 20/4 argon ion laser. This UV-capable pump laser produces up to 20 W of power and enables the ring dye laser to reach the UV with the proper dye. This laser enables the dye laser to generate several tens of mW to over 1 W of power over the spectral range of interest. Given the adequate optical access provided in the P5, this laser system is capable of performing near- and far-field plume diagnostics, internal plasma diagnostics, and internal erosion measurements.

A "multiplex" LIF technique is used at PEPL that allows simultaneous measurement of three velocity components at a given location. A small fraction of the laser beam (~1 percent) is split from the main beam and passed into a wave meter. This wave meter monitors the wavelength of the laser, the mode of the laser, and the linearity of fine scale tuning. The main beam is split into three parallel beams by a coated prism. The three beams are then chopped at different frequencies to permit discrimination of the three fluorescence signals. A small fraction of one of

these beams is passed through a reference cell. The reference cell is actually an opto-galvanic cell filled with xenon gas. However, since xenon ions and neutrals are of primary interest, the cell serves as a zero velocity LIF reference for both.

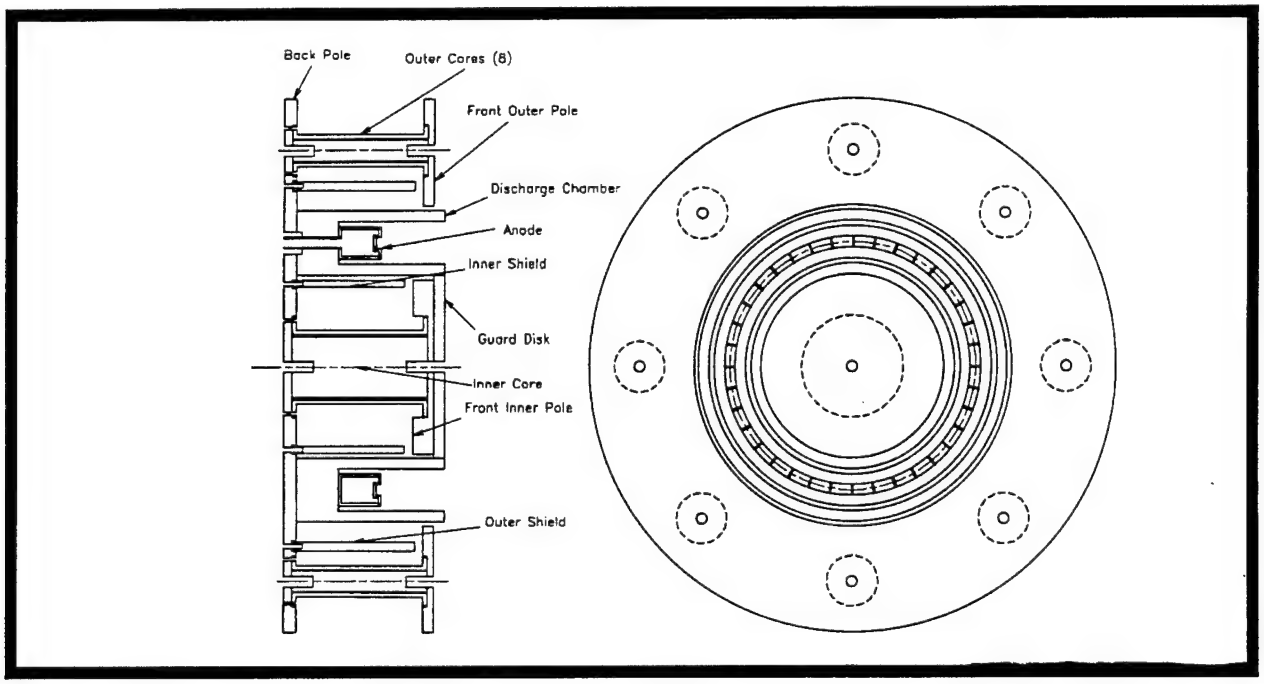

Figure 9 — Schematic of the PEPL/AFRL P5 Laboratory-model Closed-Drift Hall Thruster.

The fluorescence signal resulting from the laser beams are monitored via a monochromator coupled to a lock-in amplifier that is in phase with the chopping frequency. A reference cell also enables a rough analysis of laser beam linewidth and quality. The parallel beams are then directed to the optical port of the vacuum chamber. The parallel beams that enter the chamber are directed to a spot of interrogation by a series of mirrors and lenses mounted to a fixed breadboard. The thruster is moved about via a high-fidelity positioning system to create the spatial map. The fluorescence signal is collected via a large (8-cm-diameter) lens and mirror positioned on the same breadboard as the optics guiding the laser beams. The collected signal exits the chamber via a second port and is monitored by a monochromator that is coupled to three lock-in amplifiers, one in phase with each of the chopping frequencies. The system is aligned via optics external to the vacuum chamber and a pin (to determine the interrogation spot).

A Ti:sapphire conversion kit for the Coherent 899-29, which allows more powerful access to the near-IR, was purchased with Air Force DURIP funds. The kit has a greater tuning range than a

dye system, as well as an ability to interrogate BN (the principal erosion product of CDTs), Xe, Xe^+, and any other (as yet unspecified) transition within the 800-900 nm range.

If wavelengths corresponding to two different transitions in two different species (*e.g.*, 605.1 nm for Xe^+ and 828.0 nm for Xe) were used in the multi-plex laser configuration described above, the velocity and temperature of both species could be measured simultaneously at the same location. A high-power, single-frequency, continuously-tunable TA 100 diode laser by TUIOPTICS of Martinsried, Germany was purchased with Air Force DURIP funds, to provide this second wavelength. This particular diode laser could readily interrogate Xe, Xe^+ and any as yet unspecified transitions between 825 and 875 nm. The diode laser system's primary use would be to scan for Xe or Xe^+ and free up the dye- or Ti:sapphire-configured ring laser to scan for the second species.

PEPL has constructed and successfully demonstrated a High-speed Axial Reciprocating Probe (HARP) to allow electrostatic probe measurements within the discharge chamber of the P5 without significantly perturbing thruster operation. This is accomplished by inserting and removing probes on time scales under 100 ms to avoid probe ablation. This allows measurements to be made with very little perturbation to thruster operation; the extent of which is determined by monitoring the discharge current during probe movement. Use of the HARP with Langmuir and emissive probes causes a slight perturbation in the discharge current (less than 5% and 15%, respectively of the nominal) during all measurements. Figure 10 shows emissive probe plasma potential data taken inside the P5 with the HARP for a thruster setting of 10 A and 300 V. The narrow acceleration region is clearly seen in this figure. The HARP will continue to provide high-quality data on the interior plasma magnetic field, number density, electron temperature, floating potential, and plasma potential of the P5 at various background tank and thruster operating conditions.

All thruster performance measurements will be made with an inverted pendulum type thrust stand based on the NASA GRC design, the industry standard. In this design, a thruster is mounted to a plate that is connected to the core of a Lucas Schaevitz model 100-HR Linear Variable Differential Transformer (LVDT). The core resides within a LVDT coil that is mounted to the base of the thrust stand. Thus, the thrust stand measures the displacement of the plate due to engine thrust. The output from the LVDT is routed to a Lucas Schaevitz DTR-451 Digital Transducer Readout (DTR) and to the data acquisition system. Thruster/thrust-stand leveling is performed manually prior to chamber pump-down so that the LVDT core is in its null position within the coil. A remotely-controlled stepper motor driven pulley system is employed to provide in-situ thrust stand calibration by loading and off-loading small weights to simulate thrust. A linear curve-fit of LVDT displacement as a function of thrust is then obtained and used for performance measurements. Soon after the thruster is turned off, a post-test calibration is performed. This thrust stand has been used to measure the performance of 1 kW arcjets, the P5, and commercial 5 kW CDTs.

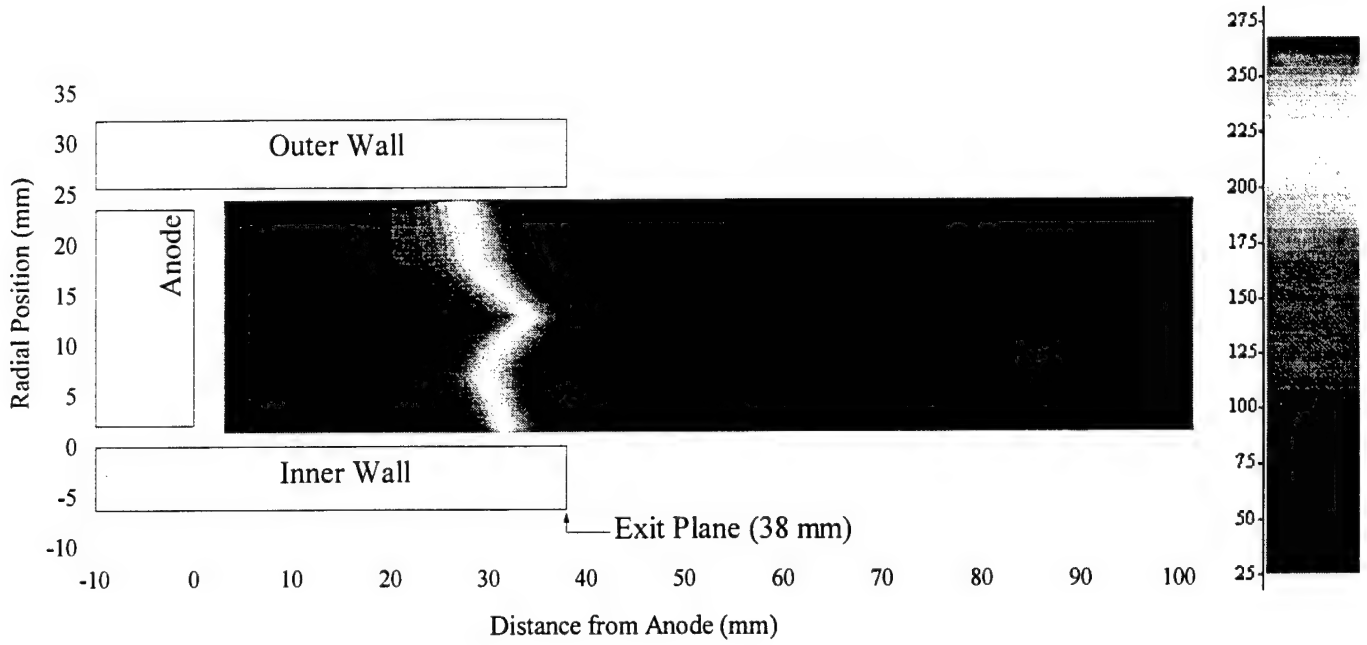

Figure 10 — P5 Plasma Potential Measurements Taken with Emissive Probe and HARP at 10 A and 300 V.

The MBMS is a time-of-flight mass spectrometer with a 45-degree parallel plate energy analyzer. It is essentially two instruments in one that when used together can give direct measurements of both ion energy and species composition. The mass spectrometer is mounted to one end of the LVTF. Ions pass into the MBMS through a sampling orifice. Two diffusion pumps are used to evacuate the MBMS in order to reduce the chance of collisions between beam ions and background gas. The beam enters the 45-degree energy analyzer, which allows ions of a specific energy-to-charge ratio to pass through and reach the detector. This ratio is selected by setting the electric field between the plates of the analyzer. By sweeping the value of this field, an entire ion energy distribution function can be determined without the need for any numerical differentiation as with the retarding potential analyzer (RPA).

For species composition, the time-of-flight mass spectrometer is used. This is the same physical system, with an electrostatic beam gate placed downstream of the sampling orifice. By pulsing the gate open and recording the time it takes for the ions to reach the detector at the end of the energy analyzer, the individual species of the plasma can be detected. This can be done because, while all of the ions passing through the analyzer for a given pass voltage have the same energy-to-charge ratio, the Hall thruster accelerates them to different velocities based on their charge state. The MBMS has been used successfully to characterize the P5 CDT and commercial Hall thrusters including the SPT-100. The MBMS will be used for making ion energy and mass spectral measurements of the P5 CDT to investigate the influence of facility pressure on each.

Ion energy measurements will also be taken with Miniature Ion Energy Analyzer (MIEA). The MIEA is a miniature version of the MBMS 45° electrostatic ion energy analyzer. While the MBMS size (2-m-long and 15-cm-diameter) is needed for time-of-flight mass spectroscopy, size is not a premium if only ion energy distribution is needed. The MIEA is 30-cm-long and 2.5-cm-diameter. Unlike the MBMS that is attached to the exterior of the vacuum chamber and has access to the plume through a gate-valved chamber port, the MIEA is placed within the chamber

and can be moved about with a conventional probe table. Given its small cross-section, the MIEA is also more amenable to near-field measurements than the MBMS or standard gridded RPAs.

History of AFOSR-Sponsored Research at PEPL

AFOSR-Sponsored Research at PEPL: 1995-1998

The centerpiece of PEPL is the Large Vacuum Test Facility (LVTF), a large vacuum chamber that was built in the early 1960s by the Bendix corporation and which was later donated to the University of Michigan in 1982 (cf. Figure 11) . This cylindrical stainless-steel clad tank, which is 9 m long and 6 m in diameter, is the largest vacuum facility of its kind at any university in the nation. Until the spring of 1998, the facility was supported by six 81-cm-diameter oil diffusion pumps backed by two 2,000 cfm blowers and four 400 cfm mechanical pumps. In addition, a Polycold PFC-1100 closed-loop refrigeration system was installed above two of the diffusion pumps to serve as a water cryopump. These pumps gave the facility an overall pumping speed of 27,000 l/s on xenon and a base pressure of $\sim 1 \times 10^{-5}$ Torr. The chamber was capable of maintaining a pressure between 4×10^{-5} Torr and 7×10^{-5} Torr during the operation of a 1.35 kW SPT-100 or D-55 TAL at 5 mg/s of xenon. Thus, the pumping system was barely adequate to characterize the intermediate-field plume of 1-kW-class CDTs and, strictly speaking, not high enough to study EMI or thruster erosion processes.

Highlights of AFOSR-sponsored research at PEPL between 1995 and 1998, through grant F49620-95-1-0331[#], include:

- Making the first measurements in the very-near-field plume of both the SPT-100[38] and D-55 TAL[39];
- Making the first 360 degree map of ion energy and mass spectra in the plume of the SPT-100[23];
- Developing and employing a number of novel plume diagnostics including a mass spectrometer, an ExB probe[40], a neutral particle flux probe[41], a heat flux probe[30], and a microwave interferometer[42];
- Making the only study of the SPT-100 plume's influence on Ku-band (17.5 GHz) and L-band (GHz) radio signals[43].

Our work on the SPT-100 was selected for the Best Electric Propulsion Paper Award for the 1998 Joint Propulsion Conference.

[#] "Spacecraft Interaction Studies with a 1 kW Class Closed-Drift Hall Thruster" [with B. Gilchrist] (4/15/95 - 4/14/98)

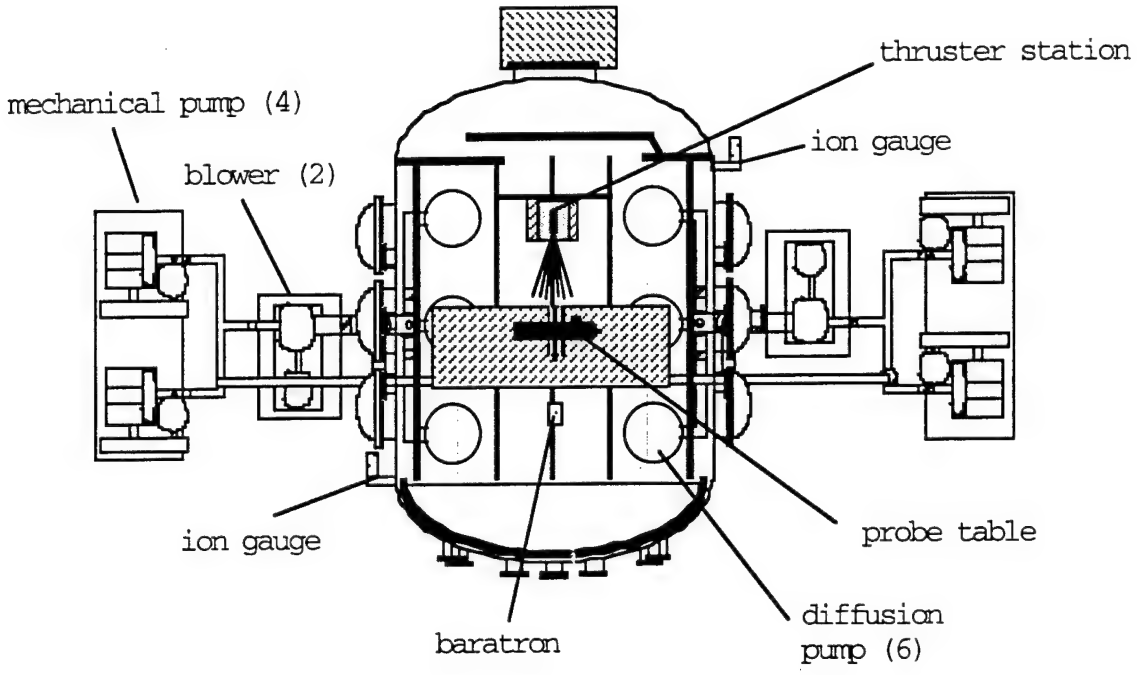

Figure 11 — The main vacuum chamber of PEPL, the LVTF (circa 1998). This 9-m-long by 6-m-diameter chamber was supported by an array of pumps, giving it a xenon pumping speed of 27,000 l/s.

1997 DURIP Award:

Although the plume characterization work was quite comprehensive, the moderate xenon pumping speed of the LVTF and the lack of laser diagnostics hampered progress. As such, a proposal was submitted to the DURIP in 1996 and awarded in 1997 entitled "Establishment of a World-Class Facility for High-Power Electric Propulsion Research," AFOSR - DoD-G-F49620-91-1-0107 (5/1/97 - 4/30/98). The proposal requested funds to purchase four TM1200 internal cryopumps and an argon-ion pumped ring dye laser.

The pumps served both to increase the xenon pumping speed of the LVTF from 27,000 l/s to 140,000 l/s, and to remove issues associated with testing CDTs in the presence of diffusion pump oil, which tends to coat thruster and probe surfaces.

DURIP funds were solicited to purchase two lasers — a pump laser and a ring dye laser — which comprise the bulk of a new laser diagnostics facility at PEPL. The Coherent model 899-29 Autoscan II ring dye laser is capable of outputting light within a spectral range of 375 nm - 900 nm (with appropriate dyes) with a linewidth of less than 500 kHz rms. The single frequency ring laser is computer controlled and has a wavelength meter attached to it that measures the laser frequency to within ±200 MHz (0.0067 cm^{-1}). This laser was selected such that if future applications should dictate (as is now the case), the laser would be capable of incorporating a

frequency doubler as well as a dye-to-Ti:sapphire conversion kit at modest cost. The dye laser is pumped by a Coherent Sabre R 20/4 argon ion laser. This UV-capable pump laser produces up to 20 W of power and enables the ring dye laser to reach the UV with the proper dye. This laser enables the dye laser to generate several hundred milliwatts of power over the spectral range of interest. A drawing of the LVTF after the 1998 DURIP upgrade is shown as Figure 12.

The combination of high pumping speed and laser diagnostics afforded by the 1997 DURIP award resulted in a tremendous increase in research capability and service to the EP community. PEPL routinely tests commercial CDTs for government and civilian entities. For example, PEPL conducted ion energy and ion current density measurements on the SPT-140 for the Air Force-sponsored IHPRPT program in September of 1999. The capability of PEPL to participate in thruster qualification activities such as these is due not only to the DURIP award, but also due to work performed under a later AFOSR program (see below).

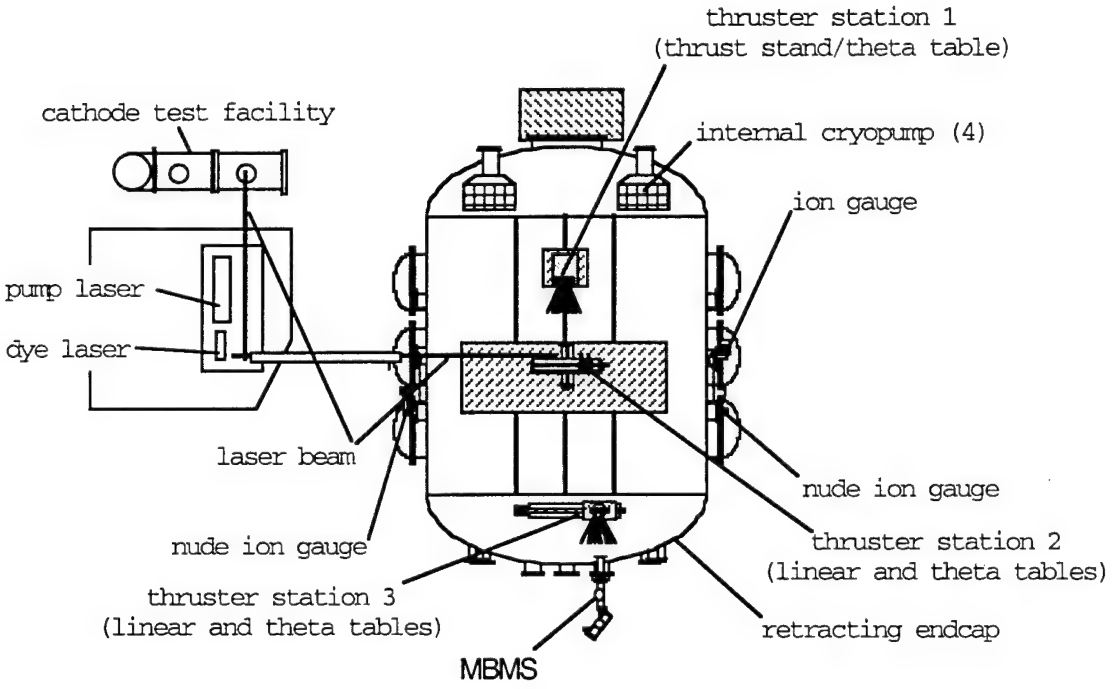

Figure 12 — The LVTF (circa 1999) is now supported by four internal cryopumps for a combined xenon pumping speed of 140,000 l/s. Also seen is the laser enclosure that contains the pump and dye laser, the cathode test facility (a 10^{-8} Torr class facility for testing cathodes and small thrusters), and the various thruster stations in the LVTF. Note that laser access is provided to both the LVTF and CTF, and that thruster station 2 in the LVTF is used for LIF engine measurements.

AFOSR-Sponsored Research at PEPL: 1998-2000

PEPL was supported by two AFOSR contracts during the 1998-2000 timeframe:

- "Development of a Field-Emitter Cathode for Low-Power Hall Thrusters," AFOSR-F49620-97-1-0380 (6/1/97 - 5/31/00); and
- "Experimental Investigations with a 5-kW-Class Laboratory-Model Closed-Drift Hall Thruster,"[&] - AFOSR - F49620-98-1-0033 (10/1/97 - 9/31/00).

The first grant was concerned with developing a propellant-less Field-Emitter Array Cathode (FEAC) for CDTs since a major stumbling block to the development of efficient low- (100-200 W) and very low-power (≤100 W) CDTs is the absence of a suitable cathode. Conventional 0.25-inch hollow cathodes consume 20 W of power and 5 sccm of propellant; more than the total propellant flow rate of a 100-W CDT. Smaller hollow cathodes (*e.g.*, 0.125-inch-diameter) are in development with the challenging goal of consuming 5 W of power. However, the minimum propellant flow rate of these cathodes is unlikely to dip much below 1 sccm. Hence, even the most advanced hollow cathode will require 50% or more of the total propellant flow rate of a 50-W CDT.

Our approach for providing electron emission for low-power CDTs was to use field emitter array cathodes (FEACs) as a replacement for hollow cathodes. The FEAC is composed of microscopic emitters attached to a conducting base plate substrate that is imbedded in layers of an insulating metal-oxide matrix. A metal grid of gate electrodes are closely placed on top of these layers so as to extract a small current from each emitter by generating a large, localized electric field at the apex of a sharpened structure (field enhancement). While the current from each emitter is small (microamps), a 1 cm^2 array may be composed of 10^6 emitters. FEACs are being actively developed around the world for use in vacuum devices, such as flat panel displays, coherent radiation sources, and ultra fast logic circuits because of their low turn-on voltages, high current densities, and stable operation in a pulsed mode.

The advantages of using FEACs are: (1) they do not require a high-power external heater; (2) they can be scaled for a variety of currents; (3) they have a high resistance to oxygen poisoning (unlike impregnated Tungsten hollow cathode inserts); (4) they require no propellant for operation; and (5) unlike filaments that also use no propellant, FEACs have the potential for long life. Unfortunately, since FEACs typically operate in high-vacuum environments ($<10^{-6}$ Torr), special care must be taken to design a cathode that is compatible with CDT ambient pressures of 10^{-5} Torr.

AFOSR AASERT funds were secured to support a graduate student for three years to investigate the use of FEAC technology with CDTs. Our emphasis was to operate a number devices, representing a wide spectrum of FEAC technologies, and measure their current-voltage characteristics and lifetimes over a wide range of pressures (10^{-10} to 10^{-6} Torr range) in an ultra high vacuum FEAC test facility.

[&] with B. Gilchrist and R. Drake.

Our initial cathode experiments in xenon environments were derived from experimental results obtained in research laboratories at SRI International and MCNC, and cathode environment characterization of a 1-kW-class laboratory-model CDT. The results obtained from experiments with single HfC and ZrC cathode tips in ~10^{-6} Torr Ar and O_2 environments showed that these materials are incredibly robust. The cathodes were not destroyed in hostile environments; often performance improved from the high-pressure exposures with operating voltages at a few thousand volts. Experiments with Mo and Si FEACs, and carbon film field emission (FE) cathodes showed that no work function increases resulted from xenon exposure. The efficiency of these cathodes was not affected by increases in pressure up to $2x10^{-5}$ Torr until the tips were damaged by ion bombardment. Si and Mo FEA cathodes were operated in xenon environments with pressures as high as 10^{-5} Torr for several hours without measurable performance degradation. Experimental results showed that FEAC performance in xenon pressures similar to those near CDT exit planes is very sensitive to operating voltages. Energy threshold values for sputtering Mo and Si targets by xenon ions were determined to be much lower than predicted. Experimental results also showed that the SRI International cathode, fabricated on a high resistivity wafer, was more resistant to arcing in high-pressure environments than other cathode configurations tested. The carbon film cathode was incredibly robust, showing no performance degradation during several hours in $2x10^{-6}$ Torr of xenon.

Another concern that was addressed, besides FEAC operation at elevated pressures, was how space-charge effects would influence FEAC operation. Modeling FEAC operation under realistic space-charge current limits showed that cathode dimensions and environment (*i.e.*, local ambient plasma parameters) play a major role in determining their performance limitations because these factors affect the configuration of the sheath. Planar sheath modeling results showed that a FEAC emitting electrons at 30 eV and positioned in the center of a Hall thruster will have a space-charge current density limit greater than ~1.7 A/cm^2. The size of the cathode can be easily scaled to provide the 1-5 A requirement of a 1-kW-class engine. A FEAC in the external position of a CDT emitting electrons at 30 eV should be able to emit at least ~60 mA/cm^2. Thus, a FEAC area of a few cm^2 will suffice for low- and very-low-power CDTs where discharge current requirements will be less than a few hundred mA.

The overall goal of the AFOSR grant that finished in August 2000 was to develop a clearer understanding of Hall thruster operating principles that can be employed to design superior engines. The key goals of the this grant include:

1) Using proven scaling relations to develop a high-performance laboratory-model CDT with a robust design that allows for access to the interior plasma with probes and laser light and yet allows for design modifications to be made with ease;

2) Perform a parametric study of how thruster operating parameters such as voltage, magnetic field strength, and magnetic field topology influence plume divergence as quantified through plume measurements; and

3) Make interior and very-near-field plume measurements with probe-, laser-, and microwave-based diagnostics to study the basic physics of this device.

To date Items 1) and 2) have been completed, while Item 3) has been initiated.

The highlights of that program include:

- Construction of a laboratory-model CDT with performance and plume characteristics equivalent to those of commercial CDTs. This engine—the P5—has performance and plume characteristics roughly equivalent to commercial engines and yet offers significant flexibility for performing internal diagnostics, for being modified, and for performing parametric trade studies;

- Very-near-, near-, and far-field, three-component laser induced fluorescence measurements in the plume of this thruster for near-instantaneous 3-D velocity and temperature determination . This is the first time that three laser beams were used to measure xenon ion and neutral velocities and temperatures at a point (1-mm-diameter spot) along three axes. Phase sensitive detection was essential in this approach. We were also the first EP laboratory to use LIF as a far-field plume diagnostic by characterizing the flowfield some 50 cm from the thruster exit plane[34];

- Internal and very-near-field electrostatic probe measurement of electron temperature, number density, and plasma potential. We developed a high-speed probe table (the fastest in the electric propulsion world) to probe the interior of the Hall thruster. The HARP (High-speed Axial Reciprocating Probe) table can place a probe in and out of a Hall thruster in 80 milliseconds (i.e., before the probe ablates). HARP provides unprecedented access to high-fidelity data inside Hall thrusters.;

- Use of Laser Induced Fluorescence (LIF) and the Molecular Beam Mass Spectrometer (MBMS) to characterize the near-field plume of the P5. Conventional wisdom states that LIF and probes give different values of ion energy spreads. This was thought to be due to the different locations of these measurements and the role charge exchange and momentum exchange collisions play in establishing the ion energy distribution in the far-field plumes where only probes had been employed. We approached this problem from both ends. We made probe measurements closer to the exit plane (1-10) cm), and made LIF measurements further from the exit plane (1-50 cm). When data from both were properly analyzed, we discovered that there was good agreement between the two in terms of characteristic ion energy (*i.e.,* where the peak in the distribution is), distribution spread, and the effective ion kinetic temperature. These findings suggest that LIF can be used as a far-field plume diagnostic tool for measuring ion energy distributions, that probes such as the MBMS can be used in the near-field to measure ion kinetic temperature of several xenon ion species, and that both probes and LIF are in agreement.

- Development of a high-frequency (34 GHz) microwave interferometer for near-field electron number density measurements;

- Applying the Resonance Probe (RP) technique to Electric Propulsion. The RP technique is one in which the potential of a modified Langmuir probe electrode is modulated by a Radio Frequency (RF) generator at various frequencies. The probe oscillation frequency is swept and resonance with the plasma is achieved when the probe potential modulation frequency reaches the local upper hybrid frequency of the plasma. Since this frequency is a function of plasma

density, the RP technique is an elegant way of measuring electron number density. We presented initial experiments with this technique at the 1999 Joint Propulsion Conference[46]. In that paper, we used the popular approach of ignoring magnetic field effects that greatly complicate the analysis. While this was justified because our RP measurements were taken in the far-field plume of the P5, we are now attempting to use the HARP system to make RP measurements within the discharge chamber of the thruster. As such, magnetic field effects cannot be ignored. Moreover, we have expanded upon the RP theory used last year to include phenomena associated with collisions and a finite electron temperature. We hope to use the new model to glean electron number density, electron temperature, and electron collision frequency from RP data.

- We are using a state-of-the-art magnetic field code to create an improved magnetic circuit for the P5 Hall thruster. We have developed a magnetic field map of the P5 thruster and used Infolytica's Magnet 6 3D magnetic field code to predict the magnetic field topology of the P5. Now that the code has been validated, it will be used to provide magnetic circuit design changes for the P5 that reduce plume divergence. The P5 will be modified to reflect design input from the code and tested for reduced plume divergence. The plume divergence testing will consist of taking the current design and operating the thruster at various magnetic field configurations. A Faraday probe will be used to make ion current density measurement sweeps up to 90° from centerline. These data have been collected for the baseline P5 design. This will be repeated once the P5 has been modified. Our hope is that a narrower ion beam cone angle will be detected with the modified P5.

- Development of a miniature, 45° ion energy analyzer for very-near- to far-field plume diagnostics. We are using Infolytica's Electnet 3D electrostatic code to improve the performance of the MIEA. The MIEA is a miniature version of the MBMS 45° electrostatic ion energy analyzer. While the MBMS has been used to characterize the plume of commercial and laboratory-model Hall thrusters with great success, its size and complexity make it difficult to export to other laboratories. While the MBMS size (2-m-long and 15-cm-diameter) is needed for time-of-flight mass spectroscopy, size is not a premium if only ion energy distribution is needed. Thus, our goal in developing MIEA was to take the ion energy analysis capability of the MBMS, but shrink it to a portable size so other laboratories can employ this technique to diagnose thruster plumes. The MIEA is just 30-cm-long and 2.5-cm-diameter. Unlike the MBMS, which is attached to the exterior of the vacuum chamber and has access to the plume through a gate-valved chamber port, the MIEA is placed within the chamber and can be moved about with a conventional probe table. Initial tests with the MIEA were promising, but later experiments showed that the device exhibited unstable characteristics in the fringes of the plume. By modeling the probe with Electnet, we were able to determine that the electric field within the device was not uniform due to its small size. We used the code to employ simple design changes that should provide extremely uniform electric fields without altering the size of the probe. We will test the modified MIEA this summer with the P5.

2000 DURIP Award:

Our most recent AFOSR award (April 1, 2000 – March 31, 2001) is the DURIP grant "Establishing a Facility For Making Non-Intrusive, Near-Real-Time Electric Propulsion Thruster

Erosion Measurements via Simultaneous Two-Frequency Laser Induced Fluorescence" F49620-00-1-0201. DURIP funds will be used to purchase three additional TM1200 internal cryopumps, a tunable diode laser, and a dye-to-Ti:sapphire conversion kit to establish a capability for making non-intrusive Hall thruster erosion measurements in near-real-time via simultaneous two-frequency laser induced fluorescence. This capability will not only enhance an already impressive vacuum facility at PEPL, but will establish a national facility where thruster erosion and spacecraft integration issues are investigated. The combination of our current ring dye laser, the diode laser, and the dye-to-Ti:sapphire conversion kit will enable the simultaneous measurement of thruster erosion products such as boron nitride or refractory metals with neutral or ionized xenon, or the simultaneous measurement of two xenon ionization states. The ability to measure both the erosion rate and the local plasma flowfield will provide unprecedented knowledge of erosion physics. Moreover, the ability to track xenon neutrals and ions simultaneously with thruster erosion products in the plume will contribute greatly to our understanding of particle transport as it relates to spacecraft surface deposition of thruster erosion products and spacecraft erosion from beam ions. A critical requirement for this capability is to have a vacuum facility of high pumping speed and sufficient volume to minimize facility effects. This will be more important and difficult to achieve as thruster size and power continue to increase. Anticipating the USAF's need for growth in thruster power, funds were requested to purchase three internal cryopumps for the 9 by 6 meter LVTF to increase its xenon pumping speed from 140,000 l/s up to 245,000 l/s. The pumps were installed in August of 2000.

References

[1] Gulczinski, F. S., and Spores, R. A., "Analysis of Hall-Effect Thrusters and Ion Engines for Orbit Transfer Missions, " AIAA-96-2973, 32nd Joint Propulsion Conference, July 1996.

[2] Sutton, G. P., Rocket Propulsion Elements, Sixth Edition, John Wiley & Sons, Inc., New York, 1992.

[3] Deininger, W. D., "Advanced Propulsion System Options for Geostationary Satellites," AIAA-94-3001, 30th Joint Propulsion Conference, Indianapolis, IN, June 27-29,1994.

[4] Jahn, R. G., Physics of Electric Propulsion, McGraw Hill Book Company, NY, 1968.

[5] Pivirotto, T., King, D., Deininger, W., and Brophy, J., "The Design and Operating Characteristics of a 30 kW Thermal Arcjet Engine for Space Propulsion," AIAA-86-1508, 22nd Joint Propulsion Conference, Huntsville, Alabama, June 16-18,1986.

[6] Curran F. M., Bullock, S. R., Haag T. W., Sarmiento, C. J., and Sankovic J.M., "Medium Power Hydrogen Arcjet Performance," AIAA-91-2343, 27th Joint Propulsion Conference, Sacramento, California, June 24-27, 1991.

[7] Carney, L. M., and Sankovic, J. M., "The Effects of Arcjet Thruster Operating Conditions and Constrictor Geometry on the Plasma Plume," AIAA-89-2723, (NASA TM-102285), presented at the 25th Joint Propulsion Conference, Monterey, California, July 10-12, 1989.

[8] Gallimore, A. D., Myers, R. M., Kelly, A. J., and Jahn, R. G., "Anode Power Deposition in an Applied-Field Segmented Anode MPD Thruster," Journal of Propulsion and Power (AIAA) Vol. 10, No. 2 March-April, 1994, pp. 262-268.

[9] Sovey, J. S., and Mantenieks, M. M., "Performance and Lifetime Assessment of Magnetoplasmadynamic Arc Thruster Technology," J. Propulsion, Vol. 7, No. 1 Jan--Feb, 1991, pp. 71-83.

[10] Patterson, M. J., "Performance Characteristics of Ring-Cusp Thrusters with Xenon Propellant," AIAA-86-90, 22nd Joint Propulsion Conference, Huntsville, Alabama, July 16-18, 1986.

[11] Aston, G., Brophy, J., Garner, C., and Pless, L., "A Xenon Ion Propulsion Module for Enhanced Spacecraft Capability," AIAA-86-1393 22nd Joint Propulsion Conference, Huntsville, Alabama, June 16-18,1986.

[12] Kaufman, H. R., "Technology of Closed-Drift Thrusters," AIAA-83-1398, 19th Joint Propulsion Conference, Seattle, Washington, June 27-29, 1983.

[13] Brown, C. O., and Pinsley, E. A., "Further Experimental Investigations of a Cesium Hall-Current Accelerator," AIAA Journal, Vol. 3, No. 5, May, 1965, pp. 853-859.

[14] Chubb, D. L. and Seikel, G. R., "Basic Studies of a Low Density Hall Current Ion Accelerator," (NASA TN D-3250), Feb.,1966.

[15] Kaufman, H. R., Robinson, R. S., Day, M. S., and Haag, T. W., "End-Hall Thrusters," AIAA-90-2595, 21st International Electric Propulsion Conference, Orlando, FL, July 18-20, 1990.

[16] Burgrova, A. I., Yermakov, Y. A., Morozov, A. I., and Yakunin, S. A., "A New Stage of Stationary Plasma Engine (SPE) Development," presented at the *Anniversary Specialist Conference on Nuclear Power Engineering in Space*, Institute of Physics and Power Engineering, Obninsk, May~15-19, 1990.

[17] Morozov, A. I., Shubin, A. P., and Elizarov, L. I., "Modern State and Future of Electric Propulsion Thrusters," presented at the *Anniversary Specialist Conference on Nuclear Power Engineering in Space*, Institute of Physics and Power Engineering, Obninsk, May 15-19, 1990.

[18] Haas, J. M., Gulczinski, F. S., Gallimore, A. D., Spanjers, G.G., and Spores, R. A., "Performance Characteristics of a 5 kW Laboratory Hall Thruster," AIAA-98-3503, 34th Joint Propulsion Cleveland, OH, July 12-15, 1998.

[19] Sankovic, J., Caveny, L., and Lynn, P. "The BMDO Russian Hall Electric Thruster Technology (RHETT) Program," AIAA-97-2917, 33rd Joint Propulsion Conference, Seattle, WA July 6-9, 1997.

[20] Martinez-Sanchez, M., "Some Thoughts on Thruster Scaling," presented at the AFOSR Workshop on Electric Propulsion for Small Satellites, Chicago, IL, May 19, 1995.

[21] Pote, B., Hruby, V., and Monheiser, J., "Performance of an 8 kW Hall Thruster," IEPC-99-080, 26th International Electric Propulsion Conference, Kitakyushu, Japan, Oct. 1999.

[22] Marrese, C., Polk, J. E., King, L. B., Garner, C., Gallimore, A. D., Semenkin, S., Tverdoklebov, S., and Garkusha, V., "Analysis of Anode Layer Thruster Guard Ring Erosion,": Proceedings of the 24th International Electric Propulsion Conference, Moscow, Russia, Sept. 1995.

[23] Gulczinski III, F. S., Examination of the Structure and Evolution of Ion Energy Properties of a 5 kW Class Laboratory Hall Effect Thruster at Various Operational Conditions, Ph.D. thesis, Dept. of Aerospace Engineering, The University of Michigan, Aug., 1999.

[24] King, L. B., and Gallimore, A. D., "Ion Energy Diagnostics in the Plume of an SPT-100 from Thrust Axis to Backflow Region," AIAA-98-3641, 34th Joint Propulsion Cleveland, OH, July 12-15, 1998.

[25] Randolph, *et al.*, "Facility effects on SPT thruster testing," IEPC-93-093, 23rd International Electric Propulsion Conference, Seattle, Washington, Sept. 13-16, 1993.

[26] Kusamoto, D., Mikami, K., Komurasaki, K., and Gallimore A. D., "Exhaust Beam Profiles of Hall Thrusters," Transactions of Japanese Society for Aeronautical and Space Sciences, Vol. 40, No.130, 1998, 238-247.

[27] Lufty, F. M., Green, A. A., Muntz, E. P., Ketsdever, A. D., "Investigation of the Operational Envelope of the CHAFF-IV Plume and Contamination Thermospheric Flow Simulator," AIAA 99-2719, 35th Joint Propulsion Conference, June, 1999.

[28] Manzella, D. H., Sankovic, J. M., "Hall Thruster Ion Beam Characterization," AIAA-95-2927, 31st Joint Propulsion Conference, San Diego, CA, July 10-12, 1995.

[29] de Grys, K. H., Tilley, D. L., Aadland, R. S., "BPT Hall Thruster Plume Characteristics," AIAA-99-2283, 35th Joint Propulsion Conference, Los Angeles, CA, June 20-24, 1999.

[30] Hofer, R. R., Walker, M. L., and Gallimore, A. D., "A Comparison of Nude and Collimated Faraday Probes for Use with Hall Thrusters," IEPC-01-20, , Pasadena, CA, October 14-19, 2001.

[31] Hofer, R. R., Peterson, P. Y., Gallimore, A. D., "A High Specific Impulse Two-Stage Hall Thruster with Plasma Lens Focusing," IEPC-01-036, Proceedings of the IEPC, Pasadena, CA, Oct 14-19, 2001.

[32] Williams, G. J., Smith, T. B., Gulczinski III, F. S., Gallimore, A. D., and King, L. B., "Correlating Laser-Induced Fluorescence and Molecular Beam Mass Spectrometry Ion Energy Distributions," Journal of Propulsion and Power, Accepted for Publication, September, 2001.

[33] Smith, T. B., Herman, D. A., Gallimore, A. D., and, Drake, R. P., "Deconvolution of Axial Velocity Distributions from Hall Thruster LIF Spectra," IEPC-01-19, Proceedings of the IEPC, Pasadena, CA, October 14-19, 2001.

[34] Haas, J. M., and Gallimore, A. D., "Experimental Investigation Of Ionization And Acceleration Mechanisms In The Hall Thruster," AIAA 2000-3422, 36th AIAA/ASME/SAE/ASEE Joint Propulsion, Huntsville, Alabama, 16-19 July 2000.

[35] Peterson, P. Y., Gallimore, A. D., and Haas, J. M., "Experimental Investigation of Hall Thruster Internal Magnetic Field Topography," AIAA-2001-3890, 37th AIAA/ASME/SAE/ASEE Joint Propulsion, Salt Lake City, Utah, 8-11 July 2001.

[36] Peterson, P. Y., Haas, J. M., and Gallimore, A. D., "Experimental Investigation of a Hall Thruster Internal Magnetic Field Topography," IEPC-01-30, Proceedings of the IEPC, Pasadena, CA, October 14-19, 2001.
[37] Hofer, R. R., Peterson, P. Y., and Gallimore, A. D., "The Effect of Vacuum Facility Backpressure on the Performance of a Hall Thruster," IEPC-01-45, Proceedings of the IEPC, Pasadena, CA, October 14-19, 2001.

[38]Kim, S. W., Foster, J. E., and Gallimore, A. D., "Very-Near-Field Plume Measurements of the SPT-100," Proceedings of the Space Transportation Symposium at the Institute of Space and Astronautical Science in Sagamihara, Japan on Jan. 13-14, 1997.
[39] Domonkos, M. T., Marrese, C. M., Haas, J. M., and Gallimore, A. D., "Very Near-Field Plume Investigation of the D55," (AIAA-97-3062): 33rd Joint Propulsion Conference, Seattle, WA, July 6-9, 1997.
[40] Kim, S. W., and Gallimore, A. D., "Plume Study of a 1.35 kW SPT-100 Using an ExB Probe," AIAA 99-2423, 34th Joint Propulsion Conference, Los Angeles, CA, June 20 - 24, 1999.
[41] King, L. B., and Gallimore, A. D., "Ionic and Neutral Particle Transport Property Measurements in the Plume of an SPT-100," (AIAA-96-2712): 32nd Joint Propulsion Conference, Orlando, FL, July, 1996.
[42] Ohler, S., Gilchrist, B. E., and Gallimore, A. D., "Microwave Plume of an SPT-100 using Xenon and Laboratory Model SPT using Krypton," (AIAA-95-2931): 31st Joint Propulsion Conference, San Diego, CA, July, 1995.
[43] Ohler, S. G., Ruffin, A. B., Gilchrist, B. E., and Gallimore, A. D., "RF Signal Impact Study of an SPT," (AIAA-96-2706): 32nd Joint Propulsion Conference, Orlando, FL, July, 1996.
[44] Haas, J. M., Gulczinski, F. S., Gallimore, A. D., Spanjers, G.G., and Spores, R. A., "Performance Characteristics of a 5 kW Laboratory Hall Thruster," AIAA-98-3503, 34th Joint Propulsion Cleveland, OH, July 12-15, 1998.
[45] Williams, G. J., Smith, T. B., Domonkos, M. T., Gulczinksi, F. S., Beal, B. E., Gallimore, A. D., and Drake, R. P., "Laser Induced Fluorescence Measurement of Ion Velocities in the Plume of a Hall Effect Thruster," AIAA 99-2424, 35th Joint Propulsion Conference, Los Angeles, CA, June 20 - 24, 1999.

APPENDIX A — A Comparison of Nude and Collimated Faraday Probes for Use with Hall Thrusters

Appendix Summary

The effectiveness of collimated Faraday probes in obtaining the ion current density profile in Hall thrusters is investigated. A collimated probe design is attractive because it offers the possibility of obtaining the true ion current density profile regardless of the facility pumping speed. The collimator is intended to act primarily as a filter for low energy ions introduced in the plume by charge exchange collisions. Experiments were conducted using a traditional nude Faraday probe and a collimated probe. The probes are evaluated using a 5 kW Hall thruster in a facility capable of maintaining background pressures of 10^{-6} Torr for flow rates of 5-10 mg/s. Detailed examination of the results has shown that the probe is interacting strongly with the plasma inside the collimator. Further study is required to bring the collimated Faraday probe to a maturity level sufficient for use in evaluating Hall thruster plumes.

Introduction

As the availability of in-space power increases, the trend in Hall Effect Thruster (HET) development is growing proportionally towards high power engines. In just the last ten years, the HET community has seen the completion of flight qualification to western standards of the SPT-100 (1.35 kW)[1-2], on-going activities for qualifying the SPT-140 (4.5 kW)[3-4], and a 1000 hour test of the T-220 (10 kW).[5] The latest trends at government laboratories sponsoring HET research are looking now towards power levels of 30-100 kW. The NASA Glenn Research Center (GRC) will be testing 50 kW engines early next year,[6] and the Air Force Research Laboratory (AFRL) has recently begun testing clusters at low power with the eventual goal of testing high power clusters.

At power levels of 30-100 kW, the mass flow rates will range from 60-200 mg/s for a 500 V thruster (compare to 4.5 mg/s in the 1.35 kW SPT-100). This will place a tremendous burden on the pumping capacities of even the largest national vacuum facilities, forcing them to operate at elevated tank pressures. These facilities include those currently in operation: AFRL's Chamber 3 (150,000 l/s on xenon), the Large Vacuum Test Facility (LVTF) at the University of Michigan (240,000 l/s), GRC's Tank 6 (400,000 l/s), and GRC's Tank 5 (2,000,000 l/s).

While there are no universally accepted guidelines on facility pressure for HET testing, Randolph, *et al.*[7] suggest that in order to characterize a HET in terms of performance, electromagnetic interference (EMI), far-field (≤1.2 m) plume properties, and life (and hence spacecraft contamination), the vacuum chamber pressure should be no more than $5x10^{-5}$, $5x10^{-5}$, $1x10^{-5}$, and $5x10^{-6}$ Torr, respectively. Since the pressures at low Earth orbit and at geosynchronous orbit are approximately $5x10^{-6}$ and $5x10^{-10}$ Torr,

respectively, a perfect simulation of pressure is not always necessary. Randolph based his analysis on free-molecular flow, arguing that below a certain chamber pressure, thruster operating characteristics are not affected by the random flux of vacuum chamber particles. Conversely, if a thruster is tested above the specified pressure, the influence of background gas being ingested into the engine through free-molecular flow must be taken into account when analyzing test data.

In Table A1 estimates of the tank pressures for several facilities show that operation in the 10^{-5} Torr range will be common for 50-100 kW thrusters, even approaching 10^{-4} Torr. Only GRC's Tank 6 meets Randolph's criteria at 200 mg/s. Given the cost of adding pumping speed to a facility – between $1-4 l/s – and the fact that most facilities are filled to capacity with cryosurfaces already, it is unlikely that significant pumping speed improvements will take place in the near future. This raises considerable questions about the reliability of the performance and plume measurements that will be taken for high power HETs. As a result, there is a growing need in the United States to develop the necessary methodologies and diagnostics to test these thrusters at elevated pressure levels so that the results are applicable to on-orbit performance. To those ends, the University of Michigan's Plasmadynamics and Electric Propulsion Laboratory (PEPL) has embarked on a program seeking to more fundamentally understand facility effects introduced by elevated backpressures. These include a recent characterization of the performance of the P5 HET at different pumping speeds.[8] This paper reports on an effort to evaluate the use of a nude versus a collimated Faraday Probe in the collection of ion current density in HET plumes.

Table A1 — Estimated tank pressures at several national facilities at 100 and 200 mg/s.

	Pressure (Torr)			
	AFRL	UofM	GRC-T6	GRC-T5
100 mg/s	9.5E-05	6.0E-05	3.5E-05	7.0E-06
200 mg/s	1.9E-04	1.2E-04	7.0E-05	1.4E-05

Faraday Probes

Plume impingement with critical hardware is the most challenging issue facing Hall thruster integration onto current spacecraft. To provide adequate predictions of the plume impact on spacecraft, several numerical sputtering model codes have been developed. Inputs to such models are typically the ion energy and ion current density distribution functions, which are experimentally determined as a function of angle with respect to the thruster centerline. Normally, the ion current density distribution has been measured with a nude Faraday probe.

A shortcoming of nude Faraday probes is that the measured ion current density depends partly on the facility size and operating pressure. This makes for questionable comparisons between ion current density data collected in different tanks, almost all of which differ considerably with respect to design and pumping speed. These differences are driven by resonant charge exchange (CEX) collisions of directed plume ions with the

random background population of neutrals. In resonant CEX collisions, a "fast" moving ion exchanges an electron with a "slow" moving neutral. Because the process does not involve momentum transfer, the resulting products are therefore a fast neutral and a slow ion with a random velocity distribution.

CEX collisions have been shown by Manzella to largely affect the measured current density profiles at angles greater than 30 degrees from thruster centerline. The data from this study is shown in Figure A1. Manzella considered the change in the current density profiles by changing the facility pressure for a constant thruster flow rate. He observed that the sharply peaked central core of the distribution was maintained for all pressures, but at angles in excess of 30 degrees, that the slope of the current density would abruptly increase. The magnitude of this increase was found to decrease with a decrease in pressure.

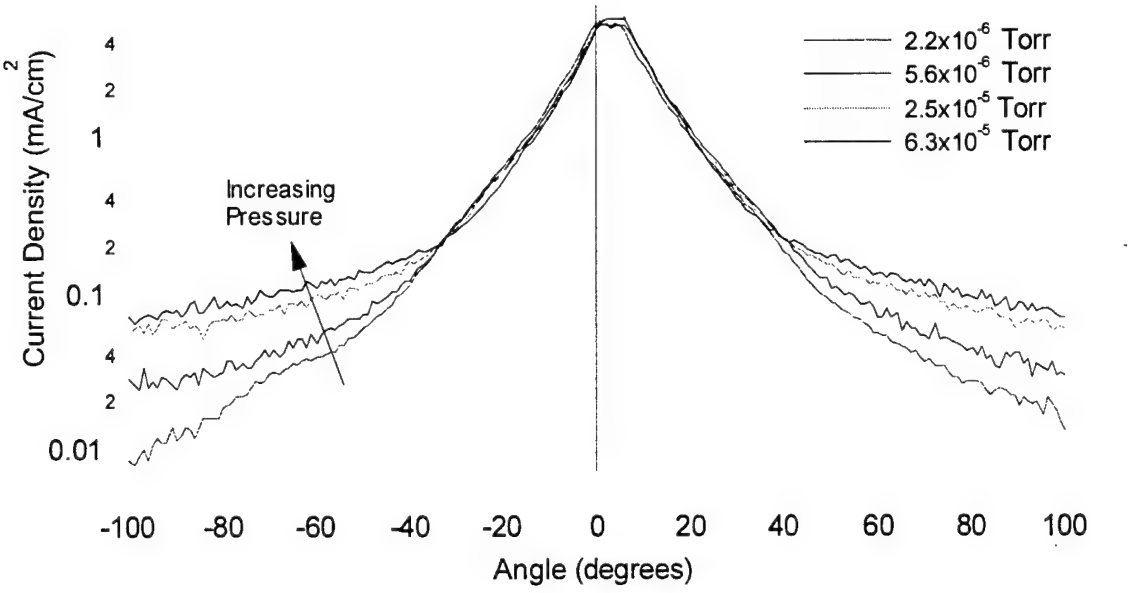

Figure A1 — Data obtained by Manzella in Ref. 9 on the SPT-100 at several chamber operating pressures.

These trends have been attributed to CEX collisions in the plume, which may occur near the thruster exit plane where the products are subsequently accelerated or at other locations of the plume where the electric field is negligible. Exit plane CEX products are most likely present in the space environment, as these collisions are in regions where the neutral density from the anode is still relatively high. Plume CEX products, however, are believed to be caused primarily by the facility background gases and should therefore be excluded from a current density measurement, which a nude Faraday probe is incapable of doing. The effects of plume CEX products are the most evident in the perimeter, where they lead to an increase in the measured current density. This seems contradictory, as the ion from a CEX collision moves at a much reduced velocity than the original fast ion. So it would seem that an electrode collecting ion current should register a lower current. Haas has recently provided an explanation for this effect.[10] Since the collector electrode of a Faraday probe is typically biased 20 V below ground to repel electrons, it

may act as a point source potential sink to low-energy CEX ions in the perimeter of the plume where the plasma density is smallest and hence the sheath thickness is greatest. Thus, more CEX ions are collected in the perimeter due to the growing sheath and an artificially large current results.

A collimated probe design could possibly mitigate this effect with nude probes, i.e. provide for a method to obtain the true ion current density profile regardless of the facility background pressure. The collimated probe is constructed by adding a long tube to the existing nude Faraday probe design. The collimator is intended to act primarily as a filter for random low energy ions introduced in the plume by charge exchange (CEX) collisions. Exit plane CEX products with a directed velocity are still collected with a collimator. In theory, the collimated current density profile could then be considered the distribution that would exist on-orbit where the population of plume CEX ions is expected to be small.

De Grys, *et al.* recently reported on the theory and design of a collimated Faraday probe.[11] Their claim is that the collimator attempts to collect random ions in the plume created by CEX collisions with energies less than 20 eV. This energy threshold was chosen because it is below a typical material energy threshold for sputtering. Ions of these energies are of little interest to plume modeling efforts. In their paper, one of the conclusions from their study was that the collimator is able to obtain the true ion current density profile regardless of the pumping speed of the facility (*i.e.* in those facilities at pressures above the Randolph criteria).

The purpose of this study is to evaluate this approach for use with HETs in a vacuum facility capable of sustaining pressures below the Randolph criteria for plume characterization. Results obtained with a collimator at these pressures should give the clearest indication of the diagnostics ability to measure the true ion current density. In the following, a review of collimated probe theory is given, then a comparison of the probe design and vacuum facilities used in this study and those in Ref.11 are presented. Experimental results and discussion of current density measurements obtained at PEPL then follow. Finally, some conclusions on the capabilities of the collimated Faraday probes are offered.

Collimated Faraday Probe Theory

The collimator is a tube with a length to diameter (L/D) ratio greater than unity housing a nude Faraday probe. Figure A2 is a schematic of the collimator geometry. Figure A3 is the idealized geometry of the collimator with respect to the thruster. The thruster is modeled as two point sources (PS_1 and PS_2), to account for the annular discharge chamber. Figures A4a-b are radial and axial plane views, respectively, which label the relevant geometric quantities. These include D_{cup}, L_{cup}, L_{col}, and R, which are defined according to Figure A2. Versions of these figures and the derivation that follows appear in Ref. 11 as well. Some modifications and additions have been made to correct for omissions in that derivation as well as for clarity.

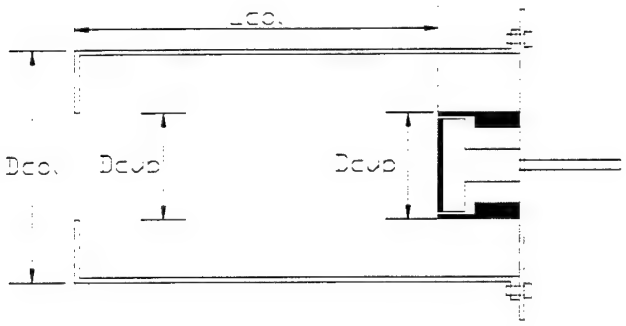

Figure A2 – Cross-sectional view of the collimated Faraday probe showing the basic geometry. Venting is through the entrance aperture or space in the rear not occupied by the nude probe and the narrow crossbar shown.

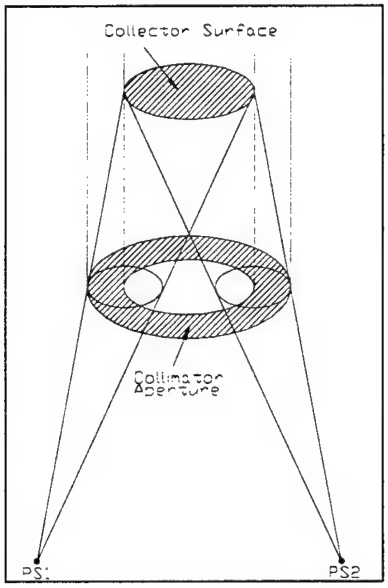

Figure A3 – Idealized geometry of the collimated Faraday probe. The thruster annular discharge chamber is modeled as two point sources (PS_1 and PS_2).

a) Radial

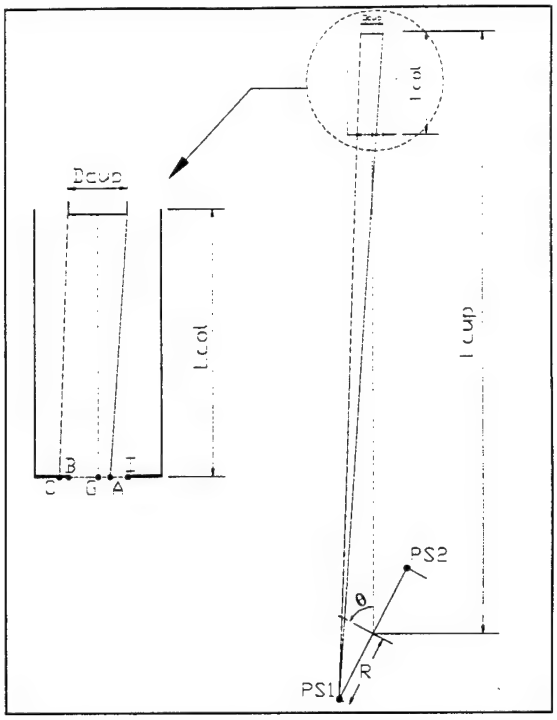

b) Axial

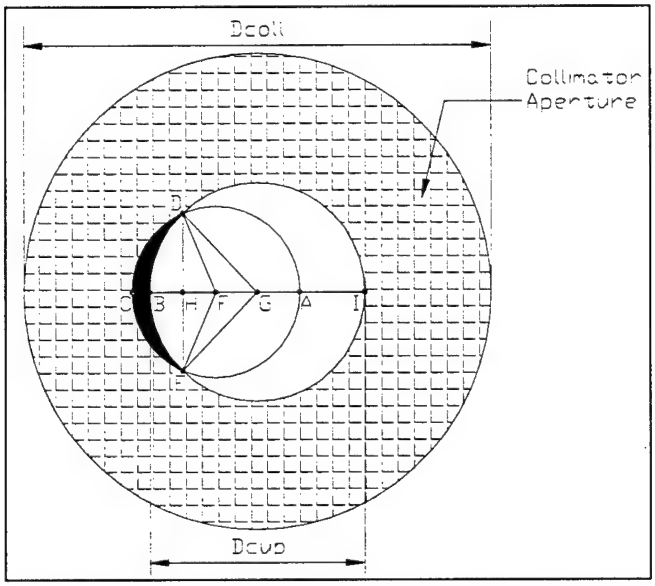

Figure A4a-b – Radial and axial plane views of the collimator geometry.

The L/D ratio significantly reduces the view factor for random CEX ions to intersect the collector face. This prohibits only those ions with velocity vectors directed within a small solid angle from entering the collimator aperture and reaching the collector where they are recorded as current. Thus, the collimator acts as a filter for low-energy, random CEX ions. Of course, the collimator also must partially block the ion beam emanating from the thruster. A scale factor is needed to account for the effect of blocking the high-energy ions that are not intended to be filtered. The scale factor is defined as the ratio of

beam current that would be collected by an uncollimated probe divided by the current collected by a collimator. Referring to Figure A5b, the scale factor for one point source is then defined as,

$$S = \left(\frac{A_{ADCE}}{A_{ADBE}} \right) = \left(\frac{A_{\phi F}}{A_{ADBE}} \right) \tag{1}$$

Where A denotes an area, and the subscripts either define a noncircular area defined by the labeled points (e.g. ADBE) or a circle defined by the center point (e.g., fF). The task remains to derive expressions for these areas as a function of angle. Because there are two point sources, the scale factors will be referred to as S_1 or S_2 as defined by the orientation of PS_1 and PS_2 in Figure A5a. S_1 and S_2 are not equal for a given angular location, instead, the functions are mirror images of each other about the centerline.

Before deriving expressions for the scale factors, consider the current density of a collimated probe. The current density contribution from each point source is related to the beam current density collected by a collimated probe as,

$$J_{coll}(\theta) = J_1(\theta) + J_2(\theta) \tag{2}$$

Where J_{coll} is the current density of the collimated probe and J_1 and J_2 refer to the current density contributed by each point source. To get the true beam current density ($J_{coll,scaled}$), the scale factor must be applied to J_1 and J_2.

$$J_{coll,scaled}(\theta) = S_1(\theta)J_1(\theta) + S_2(\theta)J_2(\theta) \tag{3}$$

How much J_1 and J_2 contribute to $J_{coll,scaled}$ is not known, so to use a collimated probe it will be necessary to equate S_1 and S_2 by another function called S_{avg},

$$\begin{aligned} J_{coll,scaled}(\theta) &= S_1(\theta)J_1(\theta) + S_2(\theta)J_2(\theta) \\ &\approx S_{avg}(\theta)\left(J_1(\theta) + J_2(\theta)\right) \end{aligned} \tag{4}$$

It will be shown later that the maximum difference between S_1 and S_2 in this study is 2.1%, so the error of equating S_{avg} for S_1 and S_2 is acceptable. Accordingly, S_{avg} must be the average of S_1 and S_2,

$$S_{avg}(\theta) \approx S_1(\theta) \approx S_2(\theta) \approx \frac{S_1(\theta) + S_2(\theta)}{2} \tag{5}$$

It is now possible to begin deriving expressions for the scale factors. The derivation will consider PS_1 and PS2 simultaneously, making note of the differences as the derivation proceeds. Recalling Eq. 1 above, the derivation begins by obtaining the area of circle F, A_{fF}, which is given by,

$$A_{\phi F} = \pi (AF)^2 \tag{6}$$

Where AF refers to the length of the line segment connecting points A and F. A similar convention will be employed for other line segments. To obtain AF, expressions for BI, BC, and AI are needed because,

$$AF = 2(AC) = 2(BI + BC - AI) \tag{7}$$

BI is simply the aperture diameter, which is equal to the collector diameter or twice the radius,

$$BI = D_{cup} = 2R_{cup} \tag{8}$$

Using similar right triangles, BC and AI can be calculated from the geometry in Figure A5a.

$$BC = \left(\frac{Lcol}{Lcup \pm R\sin\theta}\right)\left(R\cos\theta - R_{cup}\right) \tag{9}$$

$$AI = \left(\frac{Lcol}{Lcup \pm R\sin\theta}\right)\left(R\cos\theta + R_{cup}\right) \tag{10}$$

Where the positive sign in Eqs. 9-10 refers to PS_1 and the negative sign to PS_2. The expressions for BC and AI are valid for all angles ±90° from centerline, which is the range of angles for which the scale factor has physical meaning. The scale factor is considered valid so long as there is an unobstructed line of sight from the thruster to the collector. The point at which the point sources are obstructed occurs at angles slightly less than 90° in this study. BC actually becomes negative around 81° in this study, reflecting the fact that the scale factor is equal to unity at greater angles. This is because the collector is no longer overlapping the collimator face. Negative values for BC are still valid, this just reflects that point C is to the right of point B (opposite shown in Figure A5b). AI always maintains positive values over the range of angles considered. Substitution of Equations 8-10 yields an expression for A_{fF},

$$A_{\phi F} = \pi R_{cup}^2\left(1 - \frac{Lcol}{Lcup \pm R\sin\theta}\right)^2 \tag{11}$$

Where the positive sign refers to PS_1 and the negative to PS_2. Obtaining the area A_{ADBE} is more involved than A_{fF}.

$$A_{ADBE} = A_{\phi F} - \left(A_{\Delta DFE} - A_{\Delta DGE} + 2A_{\Delta DFG}\right) \tag{12}$$

The areas $A_{\angle DFE}$ and $A_{\angle DGE}$ are the areas of the circle sectors inside the acute angle defined by the indicated points. The area of triangle DDFG is given by,

$$A_{\Delta DFG} = 0.5(DH)(FG) \tag{13}$$

The length FG is given by,

$$FG = AF - AG = AF - \left(R_{cup} - AI\right) \tag{14}$$

The x-y coordinates of point D are critical for finding the length of DH and for determining the length of FH, which will be needed later in the derivation. To determine the coordinates of point D consider the equations defining circle's F and G, with an origin for both circles at point G. The equation for the circle centered about point G is,

$$x^2 + y^2 = R_{cup}^{\ 2} \tag{15}$$

The equation for the circle centered about point F is,

$$\left(x + FG\right)^2 + y^2 = AF^2 \tag{16}$$

Solving Eq. 15 for x yields a solution valid for either PS_1 (negative root) or PS_2 (positive root),

$$x = \pm\sqrt{R_{cup}^2 - y^2} \tag{17}$$

Expanding Eq. 16, substituting in for Eq. 17, and then solving for y gives the solution for DH,

$$y = DH = \pm\sqrt{R_{cup}^2 - \left(\frac{\pm\left(AF^2 - R_{cup}^2 - FG^2\right)}{2FG}\right)^2} \tag{18}$$

The first ± on the right hand side of Eq. 18 should be taken as positive, which is applicable to either PS_1 or PS_2. The second ± should be taken as negative for PS_1 and positive for PS_2.

When BC becomes zero at approximately 81°, so does DH. At angles larger than 81°, Eq. 18 becomes imaginary because it is no longer valid (the circles are not intersecting), thus DH should be set to zero when BC is less than or equal to zero. If the scale factor were valid for all angles, DH would become non-zero once again at about 99 degrees (the angle where AI becomes zero), but this case is not considered.

Having solved for y = DH, the x-coordinate (GH) can now be found by substitution of Eq. 18 into Eq. 17,

$$GH = x = \pm\left(\frac{\left(-AF^2 + FG^2 + R_{cup}^2\right)}{2FG}\right) \tag{19}$$

Where the negative root applies to PS_1 and the positive root to PS_2.

Returning to Eq. 12, it still remains to find the area of the circle sectors DFE and DGE. These areas are given by twice the areas of sectors DFB and DGB[∀],

$$A_{\Delta DFE} = AF^2 \Delta DFB \tag{20}$$

$$A_{\Delta DGE} = R_{cup}^2 \Delta DGB \tag{21}$$

The angles DFB and DGB are given by,

$$\angle DFC = \sin^{-1}\left(\frac{DH}{DF}\right) = \sin^{-1}\left(\frac{DH}{AF}\right) \tag{22}$$

$$\angle DGB = \sin^{-1}\left(\frac{DH}{DG}\right) = \sin^{-1}\left(\frac{DH}{R_{cup}}\right) \tag{23}$$

A problem now arises with the arcsine function in Eq. 22 for angles near centerline. Near centerline, the value of FH = GH - FG is negative, that is, point H is between F and G. For these angles, the angles defined in Eqs. 22-23 are obtuse and the arcsine function does not return the correct value. This is why GH was derived above. To correct this situation, the function β is defined and used in place of Eq. 22,

$$\beta = \begin{cases} \pi - \sin^{-1}\left(\dfrac{DH}{AF}\right) & ,|GH| \le |FG| \\ \sin^{-1}\left(\dfrac{DH}{AF}\right) & ,|GH| > |FG| \end{cases} \tag{24}$$

With the equations above, the scale factor can now be written down,

$$S = \frac{\pi R_{cup}^2 \left(1 - \dfrac{Lcol}{Lcup \pm R\sin\theta}\right)^2}{\pi R_{cup}^2 \left(1 - \dfrac{Lcol}{Lcup \pm R\sin\theta}\right)^2 - (AF)^2 \beta + R_{cup}^2 \sin^{-1}\left(\dfrac{DH}{Rcup}\right) - (DH)(FG)} \tag{25}$$

Where both positive signs are taken for PS_1 and the negative signs for PS_2. Note that several other equations are needed to actually compute the scale factors.

Figure A5a plots S_1, S_2, and S_{avg}, using the dimensions for the PEPL setup for a thruster exit plane to collimator entrance aperture distance of 100 cm. Dimension for the probe and thruster are given later in Table A3. S_{avg} attains a maximum value of 1.34 on

---

[∀] Recall that the sector area of a circle is given by, $A_{sector} = 1/2\, R^2\theta$.

centerline, and is set to unity at 81°. Note how S_1 and S_2 are mirror images about the centerline.

The dependence of the scale factor with distance is shown in Figure A5b, which also includes the scale factor appropriate for Ref. 11. The scale factor reported in Ref. 11 (not shown) does not agree with the one reported here. In Ref. 11, the scale factor attains a maximum value of nearly 2.0 on centerline and linearly decays with angle. This appears to be the result of an error in computing the scale factor (the derivation here is nearly identical), and has implications regarding the conclusions of Ref. 11. The scale factor reported here using the dimensions given in Ref. 11, attains a maximum value of 1.74 on centerline and does not decay as a linear function with angle.

The dependence of the scale factor on the ratio of L_{cup}/R is also shown in Figure A5b. At the equivalent axial locations (exit plane to collimator entrance), the differences between Ref. 11 and this study are a result of using different sized thrusters. The BPT-4000 has a mean diameter of 130 mm, while the thruster in this study, the P5-2, has a mean diameter of 147 mm. The scale factor at 50 cm is also given for reference.

Figure A5c plots the difference between the two scale factors, expressed as a percentage of S_2. The maximum percentage difference at 100 cm for this study is 2.1%, and at 50 cm it is 12%. Ref. 11 reports the maximum difference as 3% for their setup, while the calculations presented here indicate that this difference is 7.4%. The differences between Ref. 11 and PEPL for the same location are again driven by the thruster size. It does not seem appropriate to use the PEPL probe and thruster at distances approaching 50 cm due to the growing differences between the scale factors and the induced error that would result. At distances approaching 50 cm a more suitable thruster size, without redesigning the probe, would be a device with a mean radius on the order of 50 mm.

Experimental Apparatus

Vacuum Facility

All experiments were conducted in the University of Michigan's Large Vacuum Test Facility (LVTF). The P5-2 was mounted at thruster station 1, as indicated in Figure A6. The LVTF is a stainless steel vacuum chamber that has a diameter of 6 m and a length of 9 m. Two 2,000 CFM blowers and four 400 CFM mechanical pumps evacuate the LVTF to moderate vacuum (30 - 100 mTorr). To reach high vacuum the LVTF is equipped with seven CVI TM-1200 re-entrant cryopumps, each of which is surrounded by a LN_2 baffle. The combined pumping speed of the facility is 500,000 l/s on air, and 240,000 l/s on xenon with a base pressure of 2.5×10^{-7} Torr. The cryopump system can be operated with any number of pumps in use. For the experiments reported here, the LVTF was operated with seven cryopumps. At the average anode flow rates investigated, 5.30 and 9.95 mg/s, and a 0.76 mg/s cathode flow the operating pressures of the LVTF was approximately 3.4×10^{-6} and 5.7×10^{-6} Torr on xenon, respectively.

a)

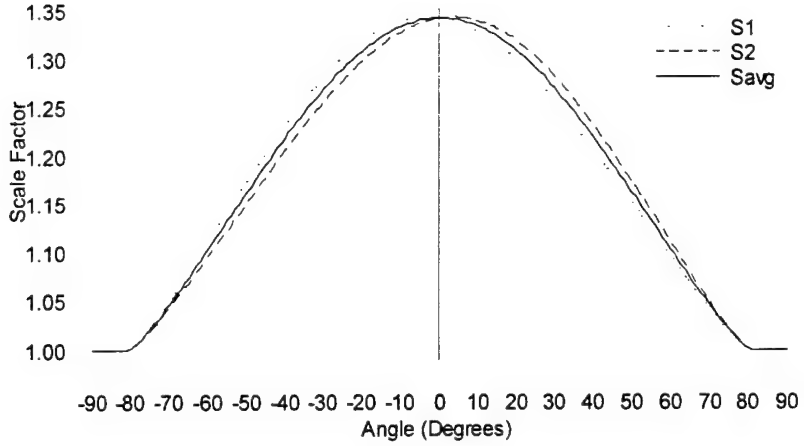

b)

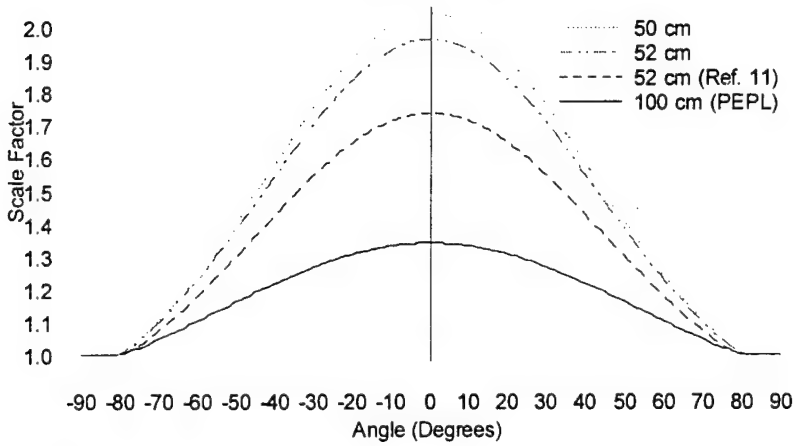

c)

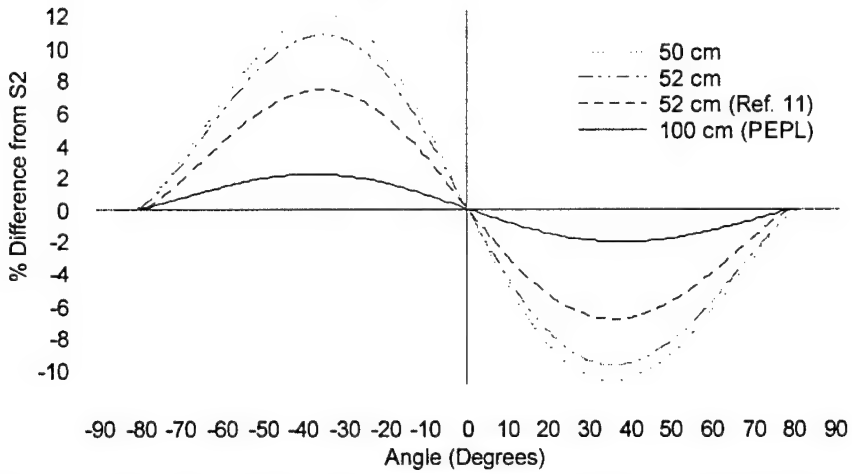

Figures A5a-c – a) The scale factor used for the PEPL probe, b) comparison of the scale factor for several thruster exit plane to entrance aperture distances, and c) the percentage difference in the scale factors for several thruster exit plane to entrance aperture distances.

Chamber pressure was monitored using two hot-cathode ionization gauges as indicated in Figure A6. The first gauge was a Varian model 571 gauge with a HPS model 919 Hot Cathode Controller. The second is a Varian model UHV-24 nude gauge with a Varian UHV senTorr Vacuum Gauge Controller. Pressure measurements from both gauges

were corrected for xenon using the known base pressure on air and a correction factor of 2.87 for xenon according to the following equation,[12]

$$P_c = \frac{P_i - P_b}{2.87} + P_b \tag{26}$$

Where P_c is the corrected pressure on xenon, P_b is the base pressure, and P_i is the indicated pressure when xenon is flowing into the vacuum chamber.

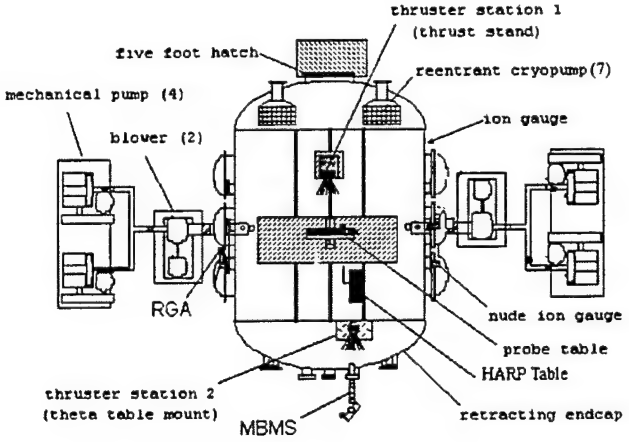

Figure A6 – Schematic of the LVTF.

For comparison, the test results presented in Ref. 11 were taken in a 2.1 m dia. X 7.2 m long stainless steel vacuum chamber, equipped with 4 cryopumps with a combined xenon pumping speed of 60,000 l/sec. Multiple ionization gauges, calibrated on xenon, where used to measure the chamber pressure. The lowest operating pressure reported was 2.3×10^{-5} Torr. The base pressure was not reported.

Hall Thruster

All experiments were performed on the P5-2 Hall thruster. A more detailed discussion of this thruster can be found in Ref. 13. This thruster is designed to operate in both single- and two-stage modes. For these experiments, the electrode used for two-stage operation was replaced with the same ceramic as the chamber walls. This enables the engine to be operated as a single-stage device. The P5-2 has a mean diameter of 147 mm, a channel width of 25 mm, and has nominal power rating of 5 kW. The thruster was allowed to operate for two hours after initial exposure to vacuum to allow for outgassing of the chamber walls. Upon subsequent thruster shutdowns and restarts, the P5-2 was operated for approximately 30 minutes before data was taken, to allow the chamber walls to reach thermal steady-state.

A lanthanum hexaboride (LaB_6) laboratory-model cathode was located at the 12 o'clock position on the thruster. The cathode orifice was located approximately 25 mm downstream and 25 mm radially away from the outer front pole piece at an inclination of 30° from thruster centerline.

The P5-2 is slightly larger in size and nominal power than the thruster in Ref. 11, the BPT-4000. The BPT-4000 has a mean diameter of 130 mm, channel width of 20 mm, and has a nominal power rating of 4.5 kW. The cathode was aligned with the thruster axis in the BPT-4000 experiments.

Faraday Probes

Both nude and collimated Faraday probes were simultaneously investigated. The collimator houses an identical nude probe. Details of the nude probe and the collimator are discussed below.

Figure A7 is a schematic of the nude Faraday probe and Figure A8 is a photograph of the probe showing the collector and guard ring. Table A2 summarizes the dimensions of both the nude probe and the collimator. The Jet Propulsion Laboratory (JPL) generously loaned PEPL the nude probes, which are identical to those used in Ref. 11. The nude probe consists of a 2.31 cm (0.91 in) diameter collection electrode surrounded on the perimeter with a guard ring. The collection electrode is aluminum that is spray-coated with tungsten to minimize secondary electron emission. The collector and guard ring are designed to be biased to the same negative potential below facility ground. This is shown in Figure A9, the electrical schematic used in these experiments. Biasing the guard ring and collector to the same potential is intended to minimize edge effects around the collector by creating a flat, uniform sheath over the collection area. The circuit shown in Figure A9 also includes a switch that allows the guard ring to be floated. The reasoning behind including this switch will be discussed in the results section later.

Figure A10 is photograph of the collimator. The collimator design is identical to the one used in Ref. 11 except for the absence of several vent holes on the main body and a different mounting scheme for the internal nude probe. The mounting scheme would not introduce any significant differences in the measurements. The vent holes were omitted here because they were not deemed necessary due to the high pumping speed of the LVTF. In addition, the vent holes could possibly introduce error by providing additional paths into the collimator interior. The vent to aperture area ratio for the Ref. 11 collimator was 5:1. In comparison, the vent to aperture area ratio for the PEPL collimator is 3.5:1. More discussion on pressure effects will be discussed below.

The use of a collimator submersed in a streaming plasma implies certain assumptions about the effects of the collimator on the local plasma. First, it is assumed that the collimator aperture is the axial location where the plume is sampled. The plasma then drifts unimpeded, i.e. free of further CEX collisions or potential gradients, into the collector. If this is not the case then the reliability of the collimator to produce meaningful results is suspect. This assumption also implies that in order to make a comparison with a nude probe, the entrance aperture of the collimator and the collection surface of the nude probe should be placed in the same axial location.

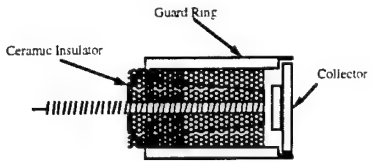

Figure A7 – Schematic of the nude Faraday probe. The collector is isolated from the guard ring with ceramic standoffs.

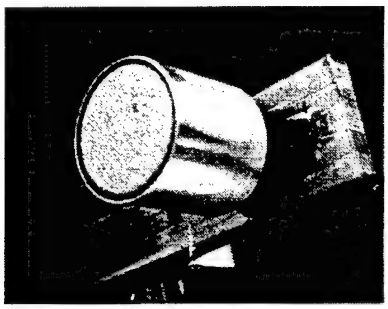

Figure A8 – Photograph of the nude Faraday probe.

Another assumption is related to the above. In Ref. 11 the collimator body is biased to the same potential as the guard ring and collector of the internal nude probe. Thus, the probe is assumed to be free of potential gradients (excluding thin sheaths) that could affect the plasma. As will be discussed below, biasing the collimator to the collector potential produces unexpected results.

Table A3 presents those values necessary to compute the scale factor applicable to this study. The dimensions are based off the thruster size, the probe position, and probe dimensions. The nude and collimated Faraday probes were positioned 11.50 ± 0.25° apart on an overhead, rotating arm that is attached to a rotary table. The probes were aligned to the center of the P5-2 exit plane and placed 100.0 ± 0.1 cm downstream of the thruster. This allowed the probes to be swept +/-100° from the thruster centerline through the plume.

A LabView VI controlled the motion of the rotary table connected to the probe arm. An 11-bit Agilent Data Logger head unit (HP34970A) with a 20-channel multiplexer (HP34901A) was used to measure the voltage drop across two 100 W current shunts (see Figure A). Measurements from both probes were taken in 1° increments, with a table angular position uncertainty of ±0.25°. The ion current density is then computed by dividing by the known probe area, the shunt resistance, and multiplying by the scale factor (for the collimated probe).

Table A2 – Dimensions of the nude and collimated Faraday probes.

Part Name	Dimension [cm (in.)]
Collimator Body	
Length	10.62 (4.180)
Inner Diameter	4.763 (1.875)
Outer Diameter	5.080 (2.000)
Nude Probe Guard Ring	
Outer Diameter	2.540 (1.000)
Thickness	0.074 (0.029)
Nude Probe Collector	
Diameter	2.31 (0.910)
Collimator Front End Cap	
Thickness	0.160 (0.063)
Inner Diameter	2.31 (0.910)
Outer Diameter	5.080 (2.000)
Support Bracket for Nude Probe	
Length	6.985 (2.750)
Width	0.318 (0.125)
Thickness	0.953 (0.375)

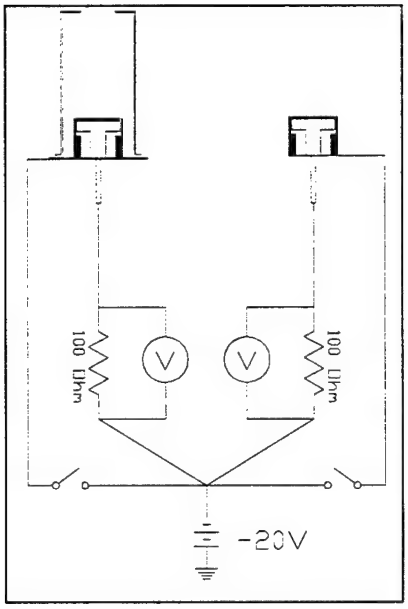

Figure A9 – Electric schematic of the nude and collimated Faraday probes. The switch allows the guard ring/collimator to float.

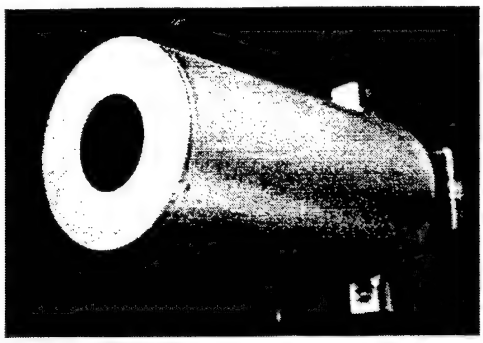

Figure A10 – Photograph of the collimated Faraday probe.

Table A3 – Probe and thruster dimensions for computing the scale factor.

Variable	Dimension [cm (in.)]
R	7.37 (2.90)
Lcup	108.0 (42.51)
Lcol	8.00 (3.14)
Dcup	2.31 (0.910)

Experimental Results

Prior use of nude probes at PEPL has indicated that a bias voltage of –20 V below ground is sufficient for the collector to enter ion saturation without substantial sheath growth. Since the collimator was a new diagnostic at PEPL, a study of the effects of the bias potential on the collected current was conducted. The probes were placed at three positions for this study: 0 or 11°, 50 or 61°, and 100 or 111°, for the collimated and nude probes, respectively. For expediency, the probes were not placed at the exact same angular location, as it was not the intent to compare nude with collimated operation. Figure A11 presents the results, which varied the bias potential up to 50 V below ground. For each position, measurements were made with the guard ring/collimator either floating or biased to the same potential as the collector.

In the following, operation of the nude probe with a floating or biased guard ring will simply be referred to as a "floating nude" or "biased nude" probe. The collector is obviously still biased to some negative potential with respect to ground. Similarly, the collimated probe guard ring/collimator will be referred to as "floating collimated" or "biased collimated" probe. Further, floating the collimator implies floating the guard ring because they are electrically connected, so for simplicity this case is referred to simply as "floating the collimator."

Consider the behavior of the nude probe first. At each angle, the nude probe behaves as expected, i.e. the floating case collects more current than biased operation and there is some collector bias where the slope of the characteristic reaches saturation.

The collimated probe characteristic only exhibits the behavior normally associated with ion saturation for the floating case. When the collimator is biased, there always exists some probe bias where the collected current is maximized. Beyond this bias, the collected current actually decreases. On centerline, the maximum current density is obtained at zero probe bias. At 50°, a peak is seen around –15 V, and at 100° the peak shifts down to less than –5 V. It is difficult to explain this behavior, but it is clear that biasing the collimator will show a non-linear angular dependence on the collected current. As a result of this study, it was concluded that the most reliable results could only be obtained with a floating collimator. Time constraints prohibited a test of floating only the collimator and biasing the guard ring and collector. Ref. 11 does not indicate attempts to investigate the probe behavior described here. The entire collimated probe in that study was biased to 20 V below ground.

As a check on the results of Figure A11, several variations to the data acquisition system were investigated. Some of these checks included: using separate power supplies for biasing the collector and collimator, biasing the nude and collimated probes separately, using handheld voltmeters to measure the shunt potentials, changing the current shunts, and verifying the isolation of the probes by measuring the impedance to ground after applying a 500 V potential (no plasma). None of these variations resulted in any changes to the measured current density.

Table A4 presents the thruster operating conditions that were investigated. The thruster was operated at 300 and 500 V and 4.5 and 10 A. Biased and floating operation was actually collected at all conditions, but not all of the biased collimator or floating nude results are presented. The excluded data showed results consistent with the observations in Figure A11 at all thruster operating conditions.

For those cases when the probes were floating, the floating potential with respect to ground was also measured. Figure A12 plots the floating potential of the nude probe guard ring and the collimated probe guard ring/collimator during operation of the thruster at 500 V, 10 A.

Figures A13 and A14 compare operation of the probes for biased versus floating operation at 500 V, 10 A. Figures 15-18 compare a biased nude probe to a floating collimated probe for all of the thruster operating conditions.

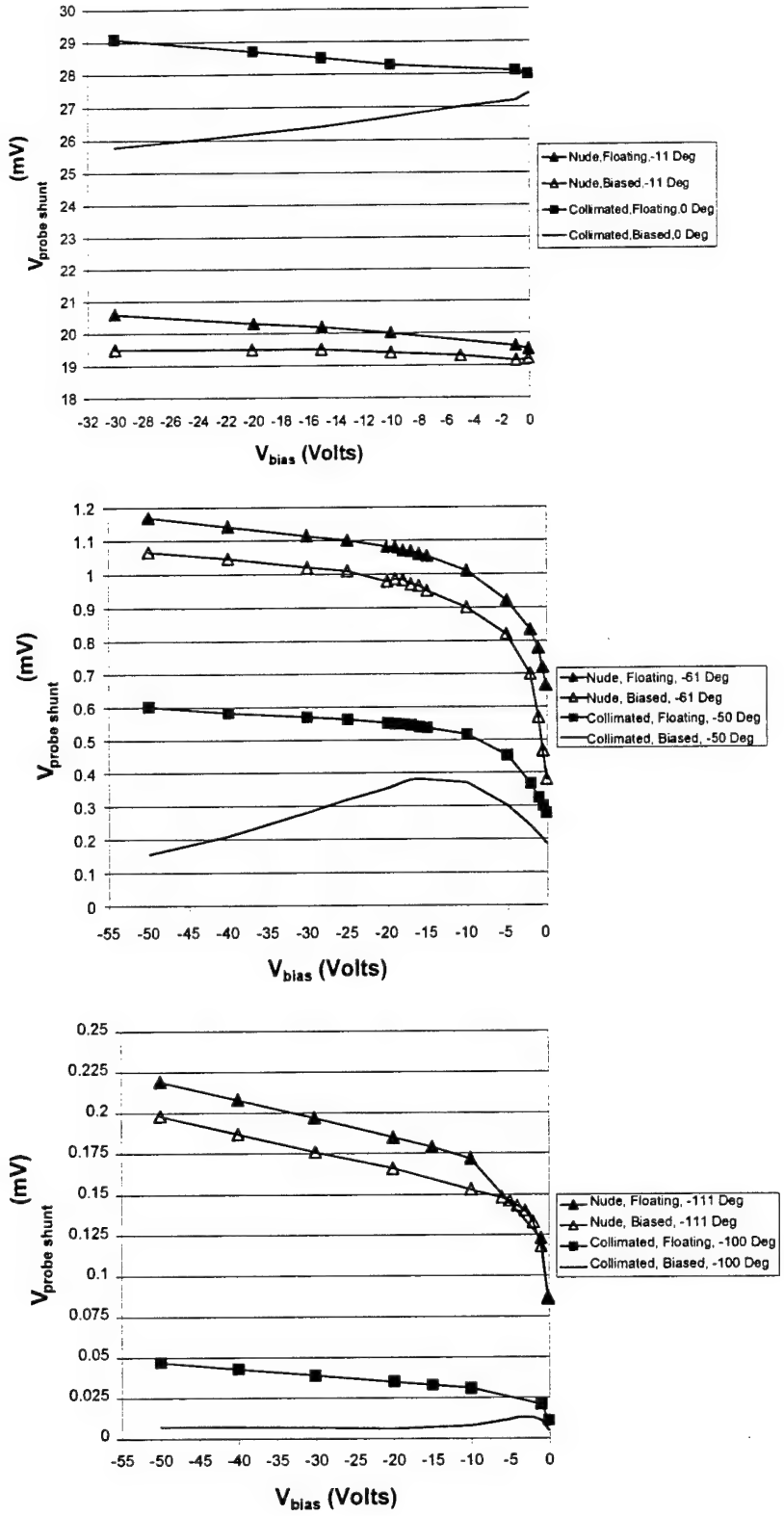

Figure A11 – Effect of varying the probe bias at several angular positions. Cases when the guard ring/collimator are biased and floating are shown. (300 V, 4.5 A thruster operation)

Table A4 – P5-2 operating conditions.

V_d (V)	I_d (A)	Anode Flow (mg/s)	Cathode Flow (mg/s)	I_{im} (A)	I_{om} (A)	V_{c-g} (V)	Pressure (Torr-Xe)	Bias (V)	Biased or Floating Guard Ring?
300	4.44	5.25	0.76	1.74	1.24	-25.7	3.4E-06	-20	Floating
300	4.46	5.25	0.76	1.74	1.24	-25.8	3.4E-06	-20	Biased
500	4.56	5.33	0.76	2.50	2.00	-21.7	3.4E-06	-20	Floating
500	4.56	5.33	0.76	2.50	2.00	-21.3	3.4E-06	-20	Biased
300	9.87	10.01	0.76	3.49	2.51	-23.8	5.7E-06	-20	Floating
300	9.87	10.01	0.76	3.49	2.51	-23.2	5.7E-06	-20	Biased
500	10.13	9.91	0.76	4.51	3.80	-22.4	5.7E-06	-20	Floating
500	10.04	9.91	0.76	4.51	3.80	-22.8	5.7E-06	-20	Biased

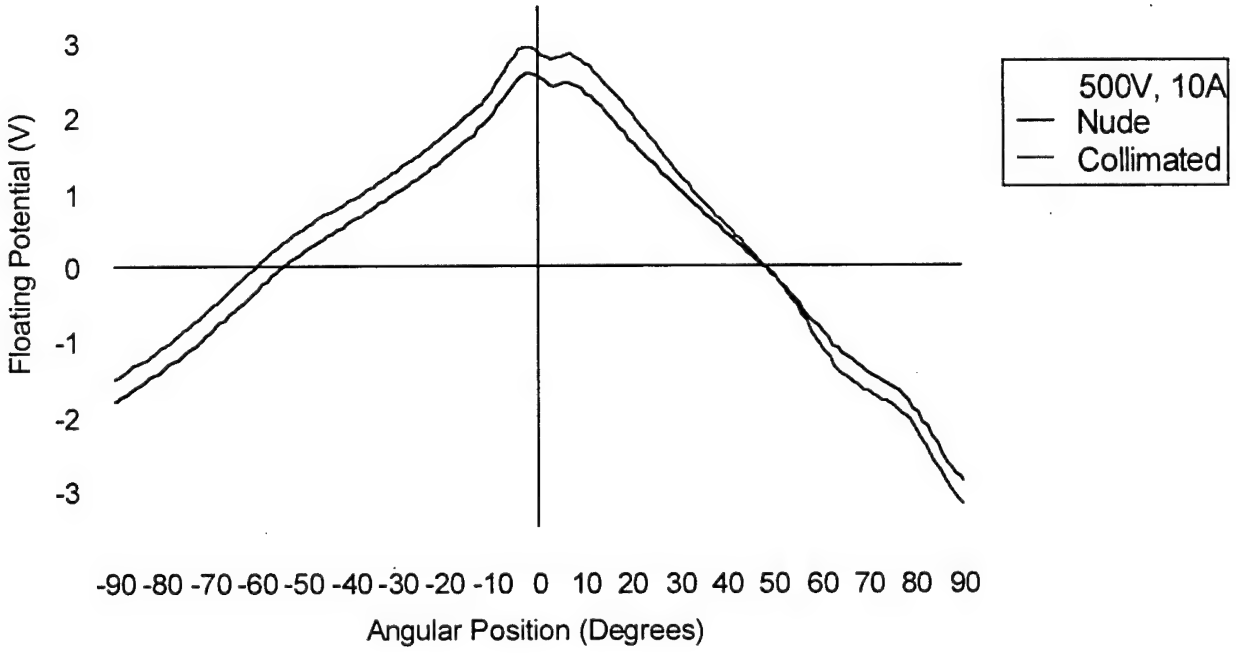

Figure A12 – Floating potential of the nude probe guard ring and collimated probe guard ring/collimator. (500 V, 10 A thruster operation)

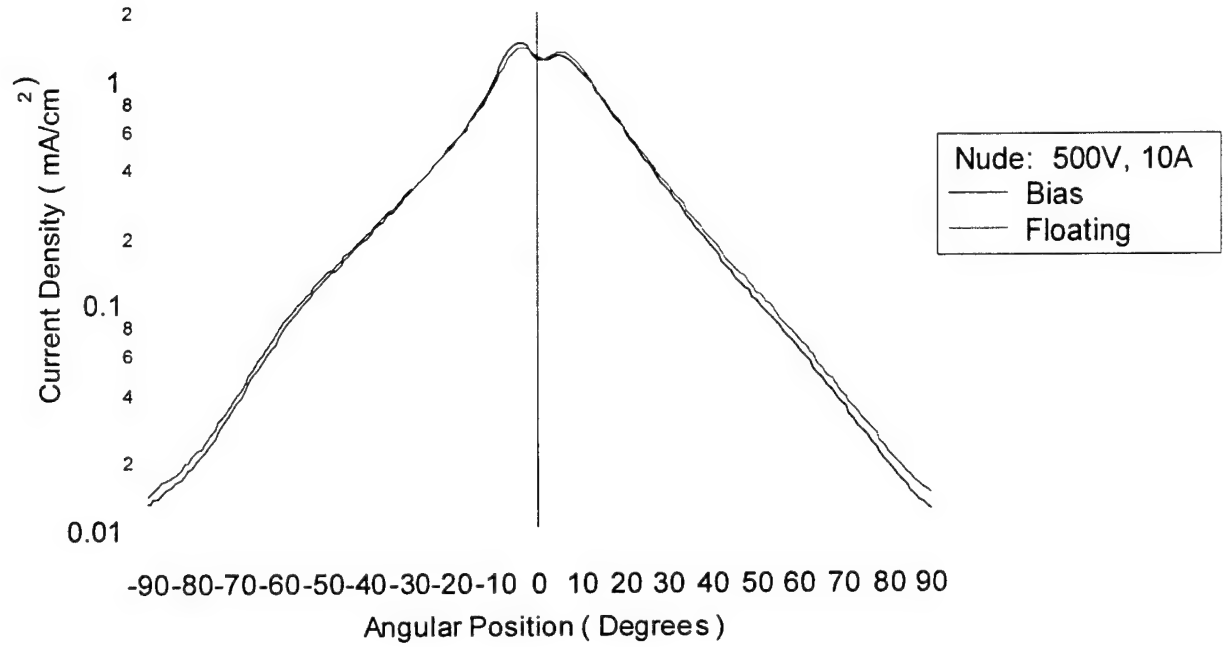

Figure A13 – Ion current density versus position for a nude probe under biased or floating operation of the guard ring. (500 V, 10 A thruster operation)

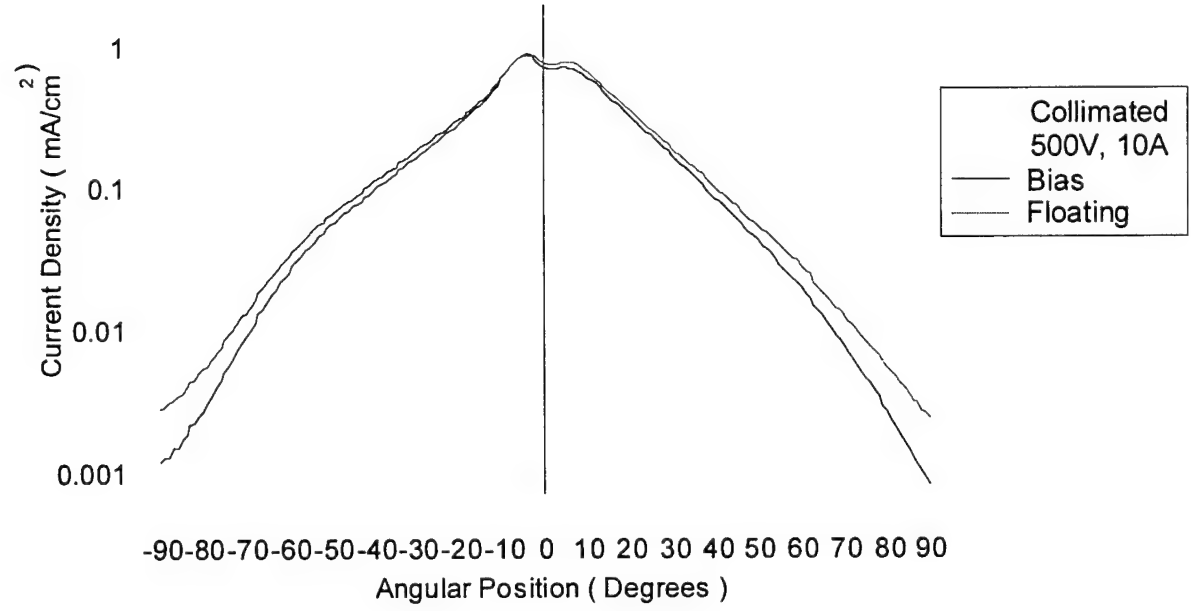

Figure A14 – Ion current density versus position for a collimated probe under biased or floating operation of the guard ring/collimator. (500 V, 10 A thruster operation)

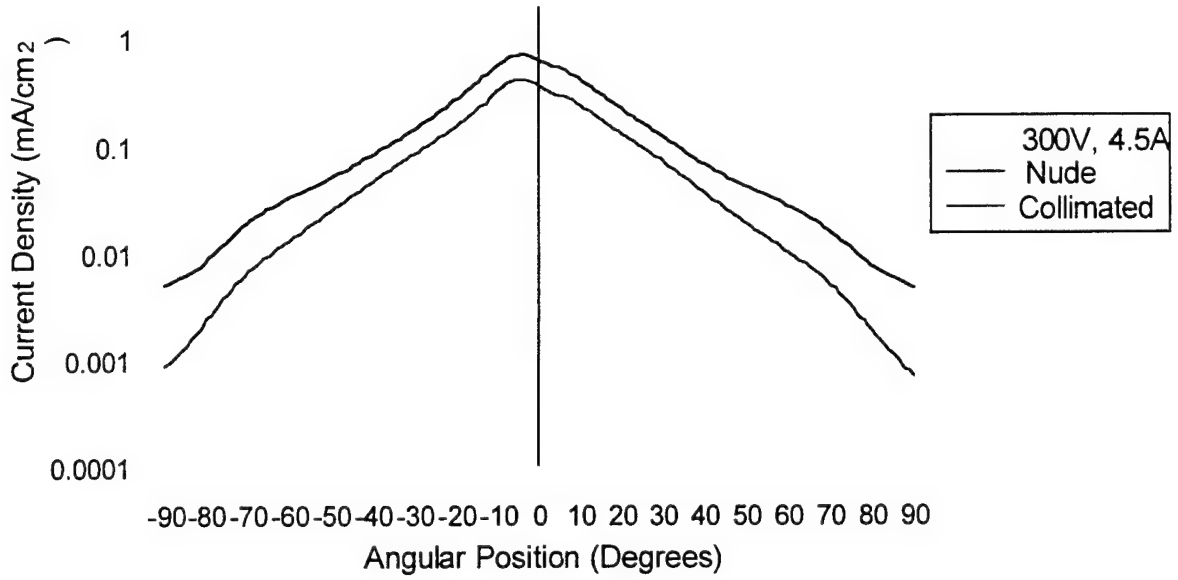

Figure A15 – Ion current density versus position for a nude and collimated probe. The guard ring on the nude probe is biased; the guard ring/collimator on the collimated probe is floating. (300 V, 4.5 A thruster operation)

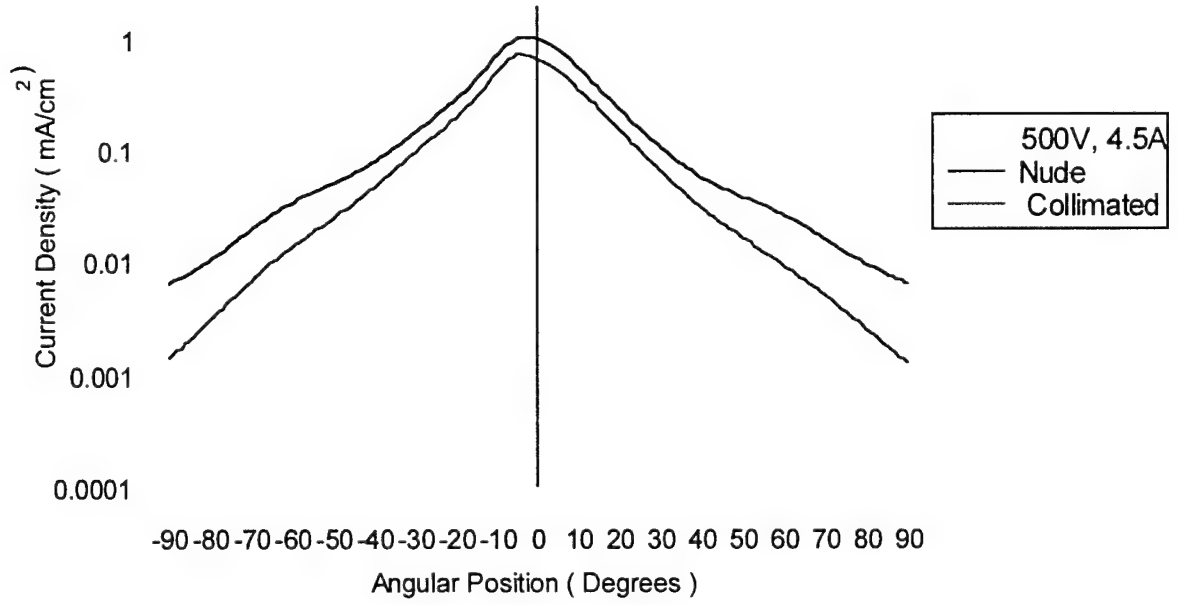

Figure A16 – Ion current density versus position for a nude and collimated probe. The guard ring on the nude probe is biased; the guard ring/collimator on the collimated probe is floating. (500 V, 4.5 A thruster operation)

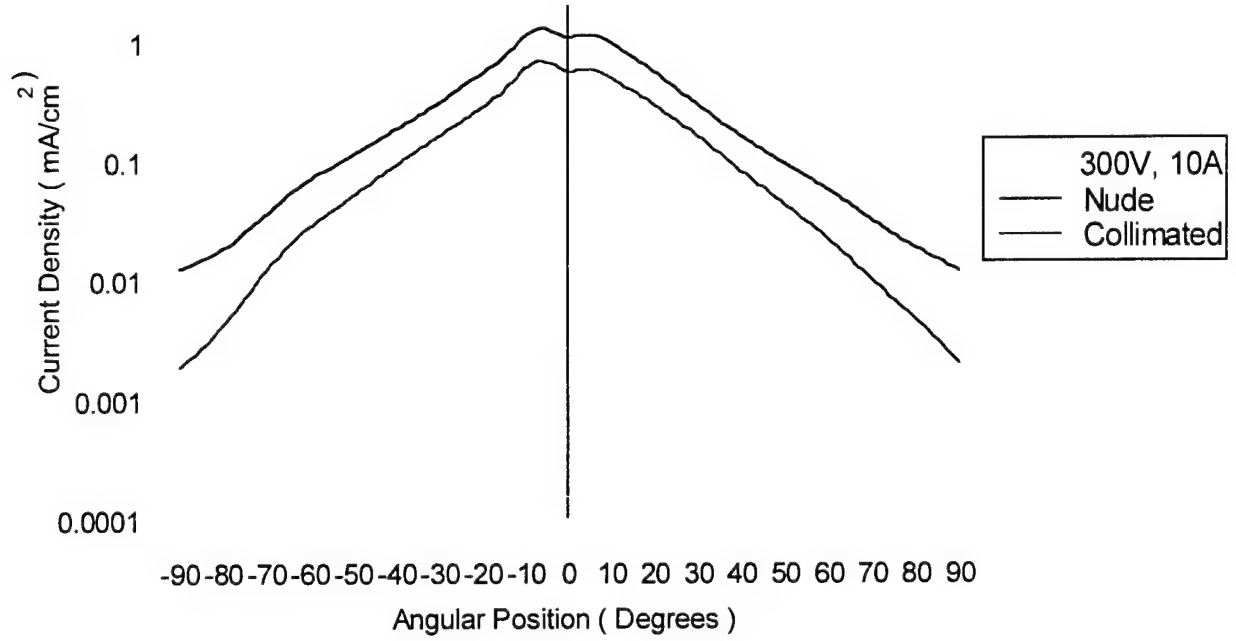

Figure A17 – Ion current density versus position for nude and collimated probe. The guard ring on the nude probe is biased; the guard ring/collimator on the collimated probe is floating. (300 V, 10 A thruster operation)

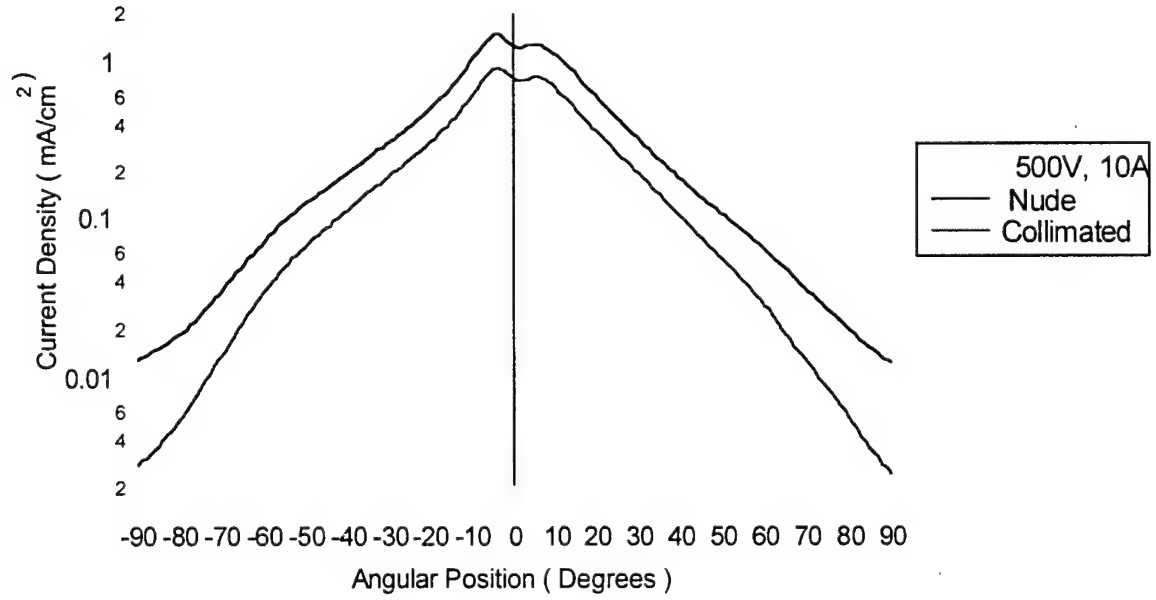

Figure A18 – Ion current density versus position for a nude and collimated probe. The guard ring on the nude probe is biased; the guard ring/collimator on the collimated probe is floating. (500 V, 10 A thruster operation)

Discussion

Figures A13 and A14, biased versus floating comparison of the same probe, show results consistent with Figure A11. The floating nude probe always collected slightly more current than for biased operation. This underscores the importance of using guard rings with nude probes to reduce error sources in the measurement. The collimated probe results in Figure A14 show that the biased case is consistently collecting less current than the floating case, especially at high angles. If the collimator is not introducing other effects in the measurement, this should not be the case. At most, the biased and floating collimator should follow each other like the nude probe behaves in Figure A13.

Referring back to Figure A1, Manzella observed that the central core of the ion current density profile was largely unaffected roughly within ±30° from centerline. Changing the facility pressure like Manzella did is analogous to the intended purpose of the collimated Faraday probe, but instead of filtering CEX products, Manzella created them. While the trends of Figure A1 may not be reproduced exactly with a collimated probe versus a nude probe, it does not seem unreasonable to expect that the two approaches (i.e. changing the pressure or using a collimator) should roughly mimic each other.

Unfortunately, this is not the case in Figures 15-18, which do not exhibit the unaffected central core shown in Figure A1. The figures consistently reveal that the floating collimator collects less current at all angles than the biased nude probe. If the biased collimator had been used, the differences would be greater. Table A5 shows the ratio of the collimated current density to the nude current density. There is a 33-48% drop between the measured current densities of the two probes (even after applying the scale factor). Some of the differences should be attributed to the collimator acting as a low energy filter for CEX ions, but it is not immediately evident how to quantify how much of the difference between the probes is a result of that filtering and not to some other process internal to the collimator. The differences could be attributed to pressure effects, potential gradients in the probe, or the scale factor itself. Some first order estimates of these possibilities will be discussed below.

Table A5 – Ratio of the ion current density for the floating collimated and biased nude probes on thruster centerline.

Condition	j_{coll}/j_{nude}
300V, 4.5A	0.58
300V, 10A	0.52
500V, 4.5A	0.67
500V, 10A	0.62

An estimate of the beam attenuation through CEX collisions is possible by considering the ion continuity equation in one dimension. After integration over some path length, z, the ratio of the initial to the final ion current density can be estimated with,[7]

$$\frac{j_z}{j} = \exp(-n_b \sigma_{ce} z) \qquad (27)$$

Where j_z is the ion current density at z, j is the initial ion current density, n_b is the background gas density, and s_{ce} is the CEX cross-section. Equation 27 is used to calculate the beam attenuation ratio over a 100 cm path length, assuming a neutral temperature of 300 K, and a charge-exchange cross-section of 55 Å^2.[14] The cross-section from Ref. 14 is only strictly valid for 300 eV ions, but it will be used here for 500 eV ions as an order of magnitude value of the true cross-section. In the calculations, recombination with electrons and higher order CEX collisions are neglected, as the mean free path's for these types of collisions is greater than a 100 cm. Table A6 shows that the beam attenuation is 6-10% at the operating pressures in these experiments, which is not enough to account for the observed differences between the nude and collimated probes. Other processes internal to the probe must be at work to account for the observed attenuation.

Table A6 – Beam current density attenuation as a result of CEX collisions over a 100 cm path length at different background pressures.

Pressure (Torr)	Attenuation
3.4×10^{-6}	0.94
5.7×10^{-6}	0.90

Another possibility is that beam attenuation is caused not by the ion transit from the thruster to the probe, but by CEX collisions inside the collimator. The ions only travel 8 cm within the collimator, so the pressure would have to be extremely high to account for this situation. Table A7 shows the internal collimator pressure required to account for the beam attenuation in Table A after adding back the attenuation for CEX collisions over the first 100 cm. The calculations indicate pressures of 2-3 x 10^{-4} Torr would be required to account for the observed differences in the probes. Such a high pressure is not likely considering the pumping speed of the LVTF and the 3.5:1 venting ratio of the collimator. A justification for why this is so unlikely is given in the following calculation.

Consider mass conservation for a control volume surround the collimator. The particle flux entering the collimator is dominated by ions because of their large directed velocities. To illustrate why this is true, typical values for Hall thruster plasmas and the background pressure were used to calculate the ratio of ion flux to neutral flux. The results showed that the ratio of ion to neutral flux was between 200-450 over the pressures and ion energies of interest. Further, assume that all ions entering the collimator are neutralized upon collision with the walls or the collector Under these assumptions, steady-state mass conservation requires that,

$$m_{Xe} n_i v_i A_{in} = m_{Xe} \frac{n_{out} v_n}{4} (A_{in} + A_{out}) \qquad (28)$$

Where A_{in} and A_{out} refer to the entrance aperture area and the space in the rear of the collimator not occupied by the nude probe, respectively. The rest of the symbols have their usual meaning. The ion velocity is obtained by assuming electrostatic acceleration

at the discharge voltage of interest. Ion density is found from the current collected by the nude probe interior to the collimator. Neutrals are assumed to be thermalized at 300 K and the exit areas are known. Under these assumptions, the internal number density of neutrals can be calculated from Equation 28 above and then expressed in terms of a neutral pressure. Table A8 presents the results of these calculations, which show that under these simplifying assumptions the internal pressure of the probe ranges from 4-8 x 10^{-6} Torr. These pressures are on the order of the background pressure in the facility during the experiments and are at least a factor of 25 lower than the pressures required if the attenuation was due to CEX collisions interior to the probe.

Table A5 – Internal collimator pressure required to account for the observed beam attenuation.

Condition	Pressure (Torr)
300V, 4.5A	3×10^{-4}
300V, 10A	3×10^{-4}
500V, 4.5A	2×10^{-4}
500V, 10A	2×10^{-4}

The previous calculations effectively rule out attenuation by high neutral pressures interior to the collimator. Two remaining possibilities are the scale factor and potential gradients interior to the probe. Error with the scale factor has already been shown to be on the order of 2% for these experiments. However, the scale factor is computed under the assumption that the Hall thruster is adequately modeled as a set of point sources. The three-dimensional nature of the thruster may be influencing the measured current somehow, but will not be considered here. There is also the possibility that the sheath around the collimator aperture is reducing the entrance area. This is unlikely because the sheath thickness likely to be encountered in the plume at 1 m results in a negligible decrease of the effective aperture area. For example, if the density is on the order of 10^{17} m^{-3} and the electron temperature is 2 eV, the Debye length is 0.03 mm. If the sheath is conservatively estimated as five times the Debye length, this reduces the aperture area only by 2%.

Table A8 – Pressure inside the collimator from mass conservation.

Condition	Collimator Internal Pressure (Torr)
300 V, 4.5 A	4×10^{-6}
300V, 10 A	6×10^{-6}
500 V, 4.5 A	7×10^{-6}
500V, 10 A	8×10^{-6}

The remaining possibility involves adverse potential gradients interior to the probe. The electric fields would be either radial electric fields that steer ions away from the collector, or axial fields that decelerate the ions so that the collected current decreases. Axial fields are extremely unlikely due to the geometry of the collimator and radial electric fields would have to persist on the order of 2-4 x 10^3 V/m to steer an ion from centerline to the

edge of the collector. This field strength equates to a potential drop of approximately 50-80 V, which is also very unlikely to exist inside the collimator. Further consideration of possible sheath effects around the collector and the sidewalls is beyond the scope of this paper.

Conclusions and Future Work

The trends observed in this investigation have led to substantially more questions than they have answered. Order of magnitude estimates have shown that the pressure inside the collimator is unlikely to account for the differences between the nude and collimated probes. Electric fields persisting throughout the collimator interior have also been ruled out. The possibility of sheath effects still affecting the measurement has not been evaluated. Clearly, further study is required to bring the collimated Faraday probe to a maturity level sufficient for use in evaluating Hall thruster plumes.

One combination that was not tested here is floating the collimator while biasing the guard ring and collector. This combination may mitigate the effects of the collimator on the plasma while still ensuring a flat sheath over the collector. Other investigations may interrogate the probe interior itself by measuring the internal pressure and plasma properties with ionization gauges and electrostatic probes. Numerical modeling of the probe is also being considered, as are alternative designs to the probe geometry and materials.

Appendix A References

1. Sankovic, J. M., Hamley, J. A., Haag, T. W., "Performance Evaluation of the Russian SPT-100 Thruster at NASA LeRC," IEPC-93-094, 23rd International Electric Propulsion Conference, Seattle, WA, Sept 13-16, 1993.

2. Garner, C. E., Brophy, J. R., Polk, J. E., Pless, L. C., "A 5,730-Hr Cyclic Endurance Test of the SPT-100," AIAA-95-2667, 31st Joint Propulsion Conference, San Diego, CA, July 10-12, 1995.

3. Hargus, W. Jr., Fife, J. M., Mason, L., Jankovsky, R., Haag, T., Pinero, L., Snyder, J. S., "Preliminary Performance Results for the High Performance Hall System SPT-140," AIAA-2000-3250, 36th Joint Propulsion Conference, Huntsville, Alabama, July 17-19, 2000.

4. Fife, J. M., Hargus, W. Jr, Jaworske, D. A., Sarmient, C., Mason, L., Jankovsky, R., Snyder, J. S., Malone, S., Haas, J., Gallimore, A., "Spacecraft Interaction Test Results of the High Performance Hall System SPT-140," AIAA-2000-3521, 36th Joint Propulsion Conference, Huntsville, AL, July 17-19, 2000.

5. Mason, L.S., Jankovsky, R.S., Manzella, D.H., "1000 Hours of Testing on a 10 Kilowatt Hall Effect Thruster," AIAA-2001-3773, 37th Joint Propulsion Conference, Salt Lake City, UT, July 8-11, 2001.

6. Jankovsky, R. S., Jacobson, D. T., Mason, L. S., Rawlin, V. K., Mantenieks, M. A., Manzella, D. H., Hofer, R. R., Peterson, P. Y., "NASA's Hall Thruster Program," AIAA-2001-3888, 37th Joint Propulsion Conference, Salt Lake City, UT, July 8-11, 2001.

7. Randolph, T., Kim, V., Kaufman, H., Kozubsky, K., Zhurin, V., Day, M. "Facility Effects on Stationary Plasma Thruster Testing," IEPC-93-93, 23rd International Electric Propulsion Conference, Seattle, WA, Sept 13-16, 1993.

8. Hofer, R. R., Peterson, P. Y., Gallimore, A. D., "Characterizing Vacuum Facility Backpressure Effects on the Performance of a Hall Thruster," IEPC-01-045, 27th International Electric Propulsion Conference, Pasadena, CA, Oct 14-19, 2001.

9. Manzella, D. H., Sankovic, J. M., "Hall Thruster Ion Beam Characterization," AIAA-95-2927, 31st Joint Propulsion Conference, San Diego, CA, July 10-12, 1995.

10. Haas, J. M., "Low-Perturbation Interrogation of the Internal and Near-field Plasma Structure of a Hall Thruster using a High-Speed Probe Positioning System," Ph.D. thesis, Dept. of Aerospace Engineering, University of Michigan, pp. 176-186, Feb., 2001.

11. de Grys, K. H., Tilley, D. L., Aadland, R. S., "BPT Hall Thruster Plume Characteristics," AIAA-99-2283, 35th Joint Propulsion Conference, Los Angeles, CA, June 20-24, 1999.

12. Dushman, S., *Scientific Foundations of Vacuum Technique*, Vol. 4, Wiley, New York, 1958.

13. Hofer, R. R., Peterson, P. Y., Gallimore, A. D., "A High Specific Impulse Two-Stage Hall Thruster with Plasma Lens Focusing," IEPC-01-036, 27th International Electric Propulsion Conference, Pasadena, CA, Oct 14-19, 2001.

14. Pullins, S., Dressler, R. A., Chiu, Y. –H., Levandier, D.J., "Ion Dynamics in Hall Effect and Ion Thrusters: Xe+ + Xe Symmetric Charge Transfer," AIAA-2000-16470, 38th Aerospace Sciences Meeting & Exhibit, Reno, NV, Jan 10-13, 2000.